Journal of Inclusion Phenomena and Molecular Recognition in Chemistry **21**: 239–282, 1995.

Photochemistry of Organic Molecules Within Zeolites: Role of Cations

V. RAMAMURTHY and NICHOLAS J. TURRO

1. Introduction

Photochemistry in organized media has attracted considerable attention during the last decade [1]. A number of materials have been utilized to "hold" molecules in a fixed orientation so as to initiate reactions. Often, such media do not remain "passive" and they themselves interact with the guest molecules and influence their photobehavior. When this occurs the material is considered to be "active" [2]. In this chapter, we are concerned with zeolites, which depending on the guest and the reaction remain either active or passive. Zeolites have been known for over two centuries and have been actively investigated by chemists with interest in their catalytic behavior for over three decades. However, photochemists' interest in such systems is only recent and can be traced to a few classic papers published in the 1980's [3]. In recent years, increasing interest in utilizing zeolites to influence the photobehavior of molecules has become evident. This chapter provides a brief summary of the work carried out in our laboratories in the area of photochemistry and photophysics of organic molecules included within X and Y zeolites. Work carried out in other zeolites is not part of this review. Although our work has been placed in a proper context with reference to the publications of others, no attempt has been made in this article to provide an exhaustive, in depth, and critical coverage of the literature [4].

The two synthetic forms of faujasite are referred to as zeolite X and Y and have the following, typical unit cell compositions [5-7]:

X type $M_{86}(AlO_2)_{86}(SiO_2)_{106}\cdot 264\ H_2O$

Y type $M_{56}(AlO_2)_{56}(SiO_2)_{136}\cdot 253\ H_2O$

where M is a monovalent cation.

Charge-compensating cations present in the internal structure of zeolites are known to occupy three different positions in zeolites X and Y. As illustrated in Figure 1, the first type (site I), with 16 per unit cell (both X and Y), is located on the hexagonal prism faces between the sodalite units. The second type (site II), with 32 in number per unit cell (both X and Y), is located in the open hexagonal faces. The third type (site III), with 38 per unit cell in the case of X type and only eight per unit cell in the case of Y type, is located on the walls of the larger supercage cavity (one unit cell consists of eight supercages). Only cations of sites II and III are expected to be readily accessible to the

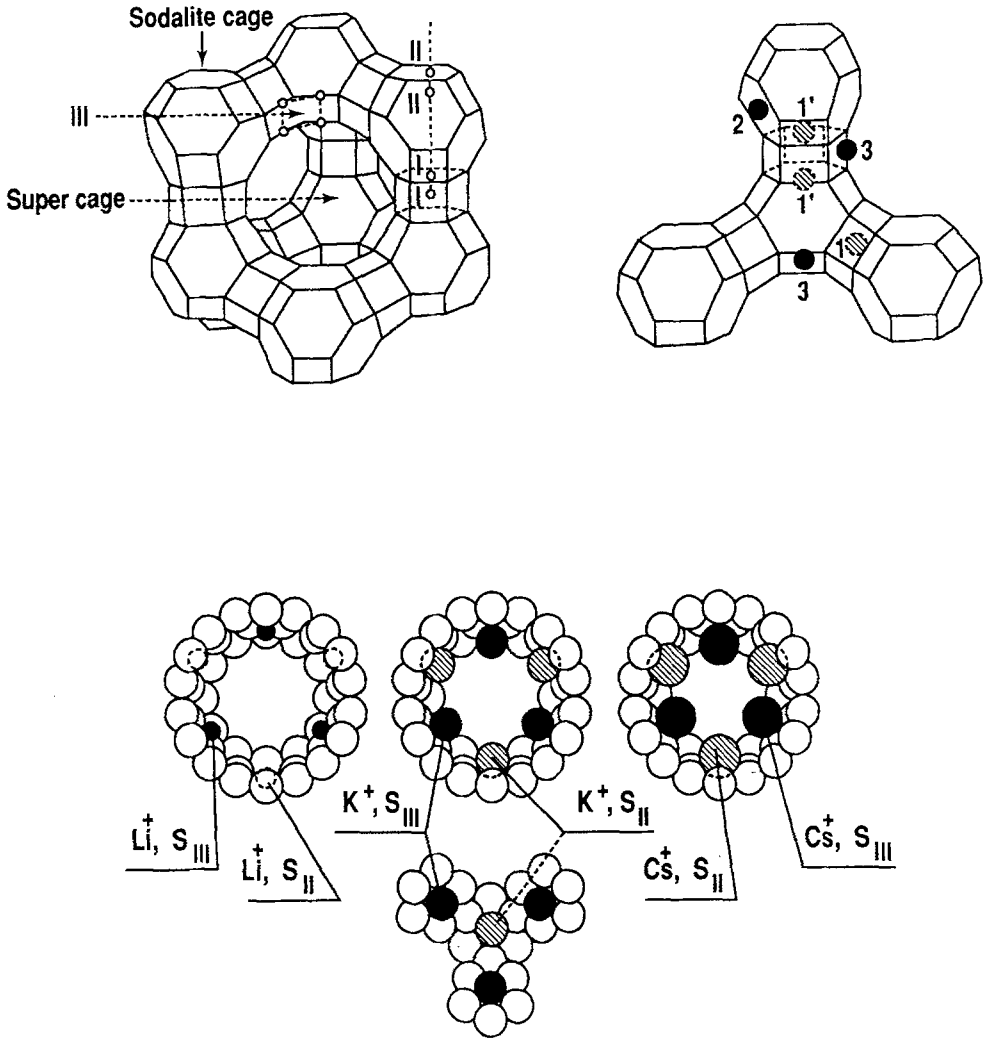

Figure 1. Supercage structure and cation location (I, II, III) within X and Y type zeolites. Bottom portion shows the reduction in available space (relative) within the supercage as the cation size increases.

absorbed organic. The free volume available for the organic within the supercage depends on the number (X vs. Y) and nature of the cations (M^+). Supercages are large as evident from their known capacity to include 28 molecules of water, 5.4 molecules of benzene, or 2.1 molecules of perfluorodimethylcyclohexane per supercage. The largest pore opening is a 12-ring with dimensions of about 7.4 Å. As the calculated supercage volumes given in Table 1 show, the free volume decreases as the cation size increases from Li to Cs [8]. The supercages form a three-dimensional network with each supercage connected tetrahedrally to four other supercages through the 12-membered ring openings.

Table 1. Cation dependence of supercage free volume in M-Y zeolites.

Cation (M^+)	Ionic Radius of the Cation (Å)[a]	Vacant Space[b] within the Supercage (Å^3)	
		Y-Zeolite	X-Zeolite
Li	0.6	834	873
Na	0.95	827	852
K	1.33	807	800
Rb	1.48	796	770
Cs	1.69	781	732

a. R. J. Ward, *J. Catalysis,* **10**, 34 (1968).

b. Calculations of polyhedral volumes were performed using a modification of the POLYVOL Program [D. Swanson and R. C. Peterson, *The Canadian Mineralogist*, **18**(2), 153 (1980); D. K. Swanson and R. C. Peterson, *POLYVOL Program Documentation*, Virginia Polytechnic Institute, Blacksburg, VA] assuming the radius of the TO_2 unit to be 2.08 Å (equivalent to that of quartz).

2. Zeolite Cavities Viewed as Nanoscopic Reaction Vessels

Recently, a simple 'model' has been adopted to understand the influence of organized media on the photobehavior of guests included in them [2,9]. As per this model, a reaction cavity is considered "*passive*" and predictions concerning the behavior of the excited guest molecules can be made solely on the bases of cavity size, shape, and flexibility when there are no significant interactions between the guest molecule and a host at various points along its walls. The cavity is considered "*active*" and predictions concerning the excited-state properties require consideration of different (and, perhaps, time-variable) interactions of the guest within the cavity when significant interaction between the walls and the guest exists. Interactions may vary from weak van der Waals forces to strong hydrogen bonds or electrostatic forces between charged centers. Presence of cations and functional groups on the surfaces of zeolites, which can interact with guest molecules, prompts the zeolites to be considered to possess "active" reaction cavities. The silica-alumina surface constituting the walls of the zeolite matrix as well as cations can participate and influence the course of photochemical and photophysical events. Thus, the zeolite cavities possess characteristics which allow them to be

classified as active cavities. However, depending on the guest molecules, the interaction between the guest organic molecules and the zeolite matrix may be so weak that one should view the zeolites as possessing "passive" reaction cavities. Examples are provided below wherein both active and passive characteristics of zeolite reaction cavities are highlighted.

3. Guest-Cation Interaction: Light-Atom Effect

Electronic interaction between the cation and the guest molecules stabilizes the guests at sites close to the cation. The strength of binding interaction between the cation and the guest molecule, as per ^2H NMR:phenanthrene in zeolite X of phenanthrene within M^+-X zeolites, is directly dependent on the charge density/electrostatic potential of the cation [10]. The higher the charge density (i.e., charge per unit volume of the cation), the stronger the binding (ΔH binding: Na^+, 14.9; K^+, 11.0; Cs^+, 7.9 kcal $mole^{-1}$). Photophysical properties of the guest molecules included within zeolites are also influenced by the cation; the nature of the influence depends on the cation. The phenomenon observed with smaller and lighter cations is termed the "light-atom effect" and is discussed in this section.

In aromatics (included within zeolites), the lowest energy symmetry forbidden electronic absorption band gains intensity with light cations [11]. Diffuse reflectance spectra recorded for pyrene, at a low loading level (Figure 2), within a number of cation exchanged X and Y zeolites suggest that the interaction between the cation and pyrene is strong and that the strength of interaction depends on the polarizability of the cation. In Figure 2, the intensity of the 0–0 transition of the S_0 to S_1 band is dependent on the charge density of the cation present within supercages. Further work is required to identify the cause of the above changes brought forth by cations. Tentatively, we believe that the symmetry reduction of the aromatic molecule occurs due to strong interaction between the cation and the aromatic along the π face resulting in slight bending of the aromatic plane.

Lifetimes of the excited singlet and triplet states of aromatics are influenced by the cations. A consistently shorter lifetime was measured in Li-X than in Na-X for the excited singlet state of a number of aromatic molecules (Table 2) [12]. It is quite likely, on the basis of what has recently been shown in the case of silica surfaces [13], that reduction in lifetime results from enhanced radiationless processes when the aromatic molecules interact strongly with the cations.

In the case of ketones, the "light-atom effect" manifests itself in altering the nature of the lowest triplet state [14]. There is a small difference in diffuse reflectance spectral maxima between Li-X– and Cs-X–valerophenone complexes. Excitation (250–300 nm) of valerophenone (VLP) included in zeolites at 77 K gives rise to phosphorescence in the region 375 to 550 nm. The emission and excitation spectra of VLP in Li-X and Cs-X are displayed in Figures 3 and 4. The triplet lifetimes for Na-, K-, and Rb-X are all

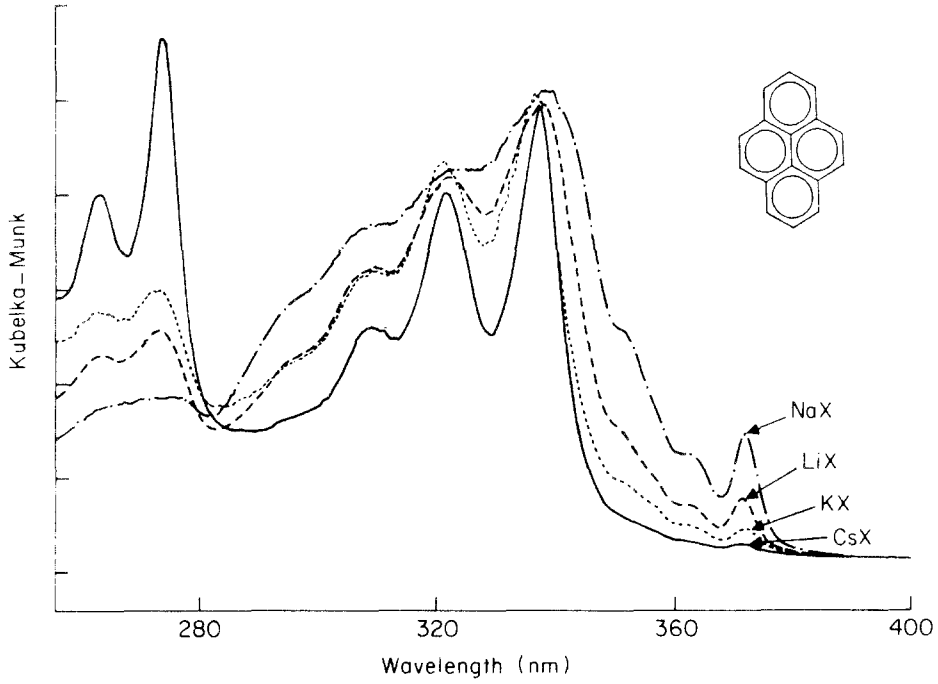

Figure 2. Diffuse reflectance spectra of pyrene included in cation-exchanged X zeolites. Note the intensity dependence of λ_{max} at ~370 nm on the cation.

Table 2. A comparison of the singlet lifetimes (ns) of aromatics in various cation-exchanged X zeolites

Zeolite	Naphthalene	Acenaphthene	Phenanthrene	Pyrene	Chrysene
Li-X	32.6	5.0	29.8	92.4	19.2
Na-X	49.1	11.6	36.6	115.4	27.1
K-X	19.4	13.1	27.8	161.4	39.2

between 0.4-1.2 μs indicating little effect of the cation, at least within the limitation of the rather large variations in triplet lifetime from one sample to the other. However, there are significant changes when the cation is changed to either Li or Cs. For the Li-X samples, the triplet decay is much longer (4–5 μs) and does not give satisfactory fits to a single exponential decay. It is quite likely that the long lifetime observed in Li-X is a consequence of the change in the character of the lowest triplet from $n\pi^*$ to $\pi\pi^*$. Such a proposal is supported by the phosphorescence spectra. Examination of Figure 3 reveals that the emission observed in Li-X is distinctly different from that in Cs-X. While the emission in Li-X is characteristic of a $\pi\pi^*$, that in Cs-X is of a $n\pi^*$ state [15]. Such a

reversal in the character of the lowest triplet is known to occur in polar solvents. The interior of Li-X being more polar [16] than other cation-exchanged X zeolites (see the section on polarity above) such a reversal is not unexpected. It should be borne in mind that part of the lengthening of the lifetime results from conformational effects, discussed briefly below.

Photolysis of several alkylphenyl ketones (Chart 1) in benzene and as complexes of zeolite M^+-X and M^+-Y (M = Li, Na, K, Rb, and Cs) gave products resulting from both Norrish type I and type II processes (Scheme 1) [17]. Results with a few ketones are illustrated in Figure 5. It is clear from the figure that the yield of benzaldehyde, a product of the Norrish type I process, is enhanced significantly within zeolites with respect to benzene. Cycloalkanones, which normally do not undergo Type I reactions in solution, upon irradiation in M^+-Y zeolites yield products resulting from Type I processes as major products (Figure 6). As illustrated with a few examples in Figure 7, the relative yield of Type I to Type II products depends on the cation; smaller cations such as Na have a larger influence.

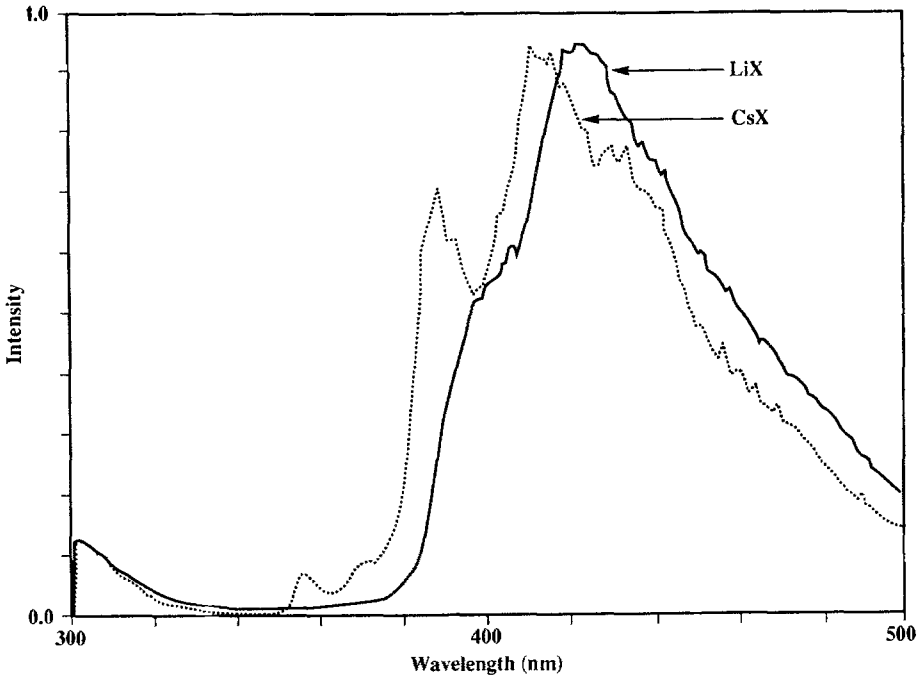

Figure 3. Phosphorescence emission spectra of valerophenone included in Li-X and Cs-X.

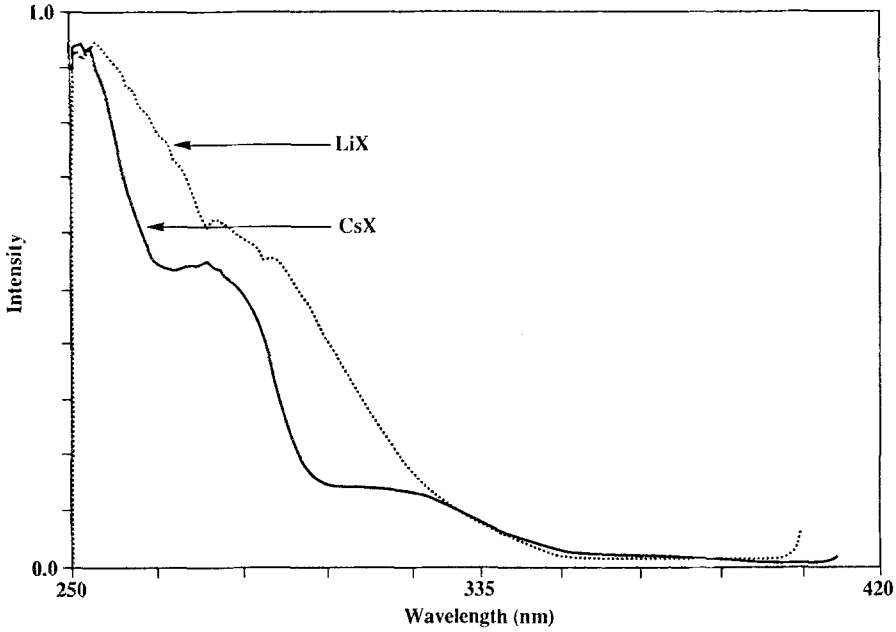

Figure 4. Phosphorescence excitation spectra of valerophenone included in Li-X and Cs-X.

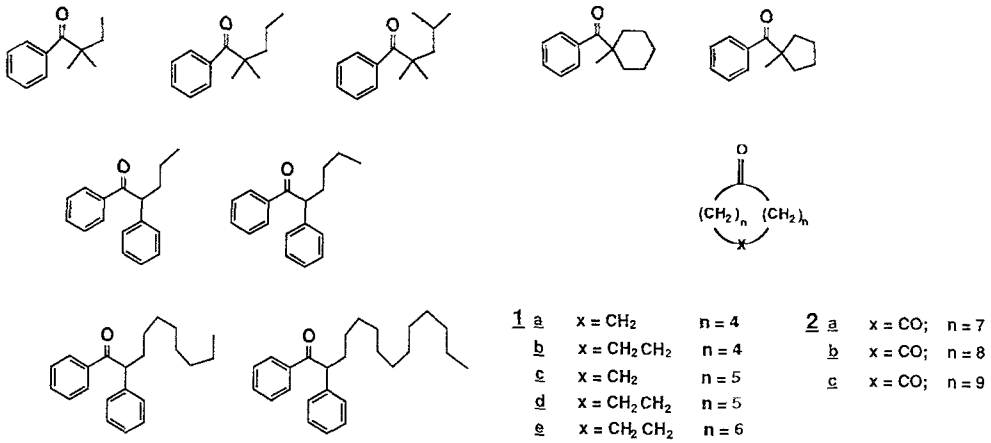

1	a	$x = CH_2$	n = 4	2	a	x = CO; n = 7
	b	$x = CH_2CH_2$	n = 4		b	x = CO; n = 8
	c	$x = CH_2$	n = 5		c	x = CO; n = 9
	d	$x = CH_2CH_2$	n = 5			
	e	$x = CH_2CH_2$	n = 6			

Chart 1.

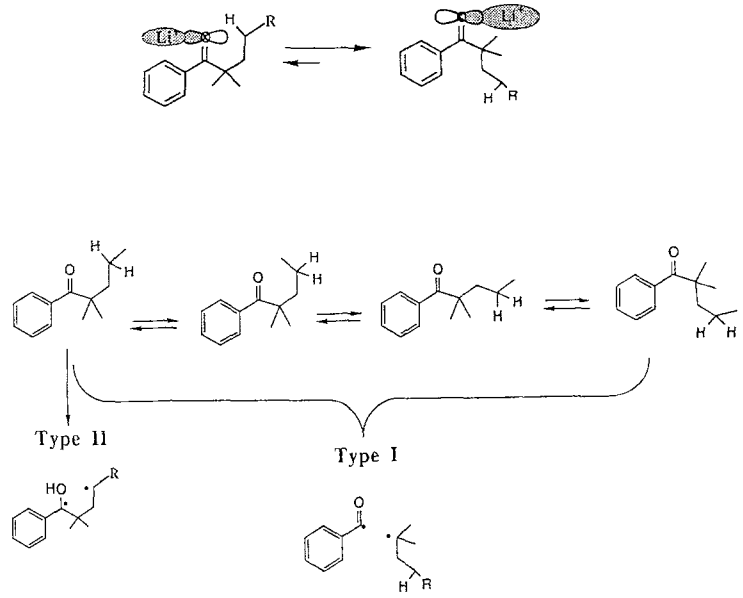

Scheme 1.

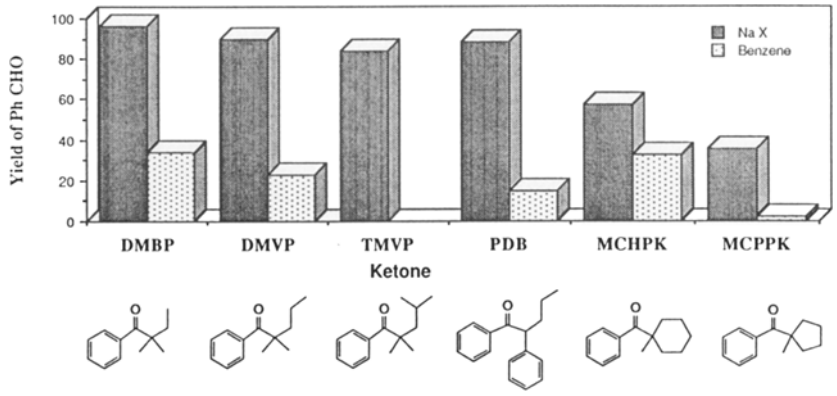

k_α	0.08	0.09	(0.09)	(0.21)	0.25	(0.25)	X 10^8
k_H	0.10	1.0	(5.0)	(1.0)	1.7	(0.25)	X 10^8

Figure 5. Type I, Type II reactivity controlled by cations within zeolite: studies with phenyl,alkyl ketones.

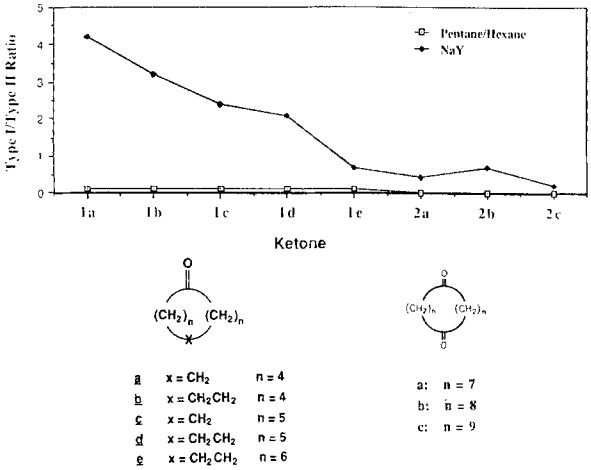

Figure 6. Type I, Type II reactivity controlled by cations within zeolite: studies with cyclic ketones.

It is proposed that the cations present within the supercage interact electronically with the carbonyl chromophore and thus, impede, sterically, the hydrogen abstraction (Scheme 1). Changes in preferred conformations are brought forth by cation binding. The effect is expected to be greater with Li^+ because it binds very strongly. Such a binding would affect the rate of hydrogen abstraction, but not the α-cleavage, and so would be expected to decrease the efficiency of the type II process alone. The mechanistic rationalization above is supported by triplet lifetime measurements for valerophenone and dimethylvalerophenone included within various cation-exchanged zeolites.

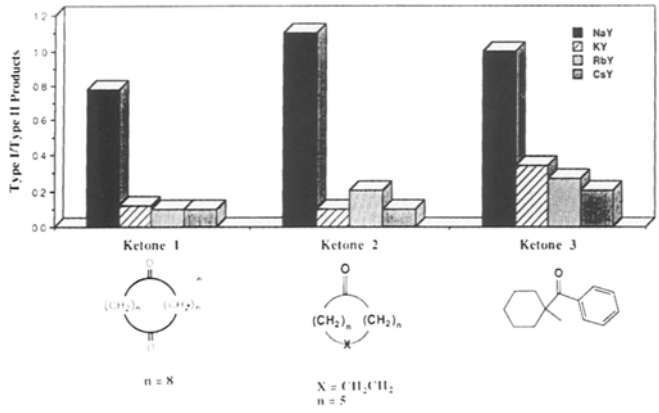

Figure 7. Dependence of type I to type II ratio on the cation. Note the higher influence by Na^+ with respect to other cations.

Another example is the photobehavior of α-alkylbenzoin ethers (X = O) and α-alkyldeoxybenzoins (X = CH_2; Scheme 2) (Table 3) [18] which provide important information. The zeolite cavity induces α-alkyl benzoin ethers to yield products derived via the type II pathway, a minor pathway in benzene. On the other hand, zeolites inhibit α-alkyldeoxybenzoins from proceeding via the type II pathway, which is favored in benzene. This is attributed to the ability of the cation present in the cavity to control the conformation of the included molecules (Scheme 2). The presence of an alkoxy chain in α-alkylbenzoin ethers most likely directs the chelation of the cation to a conformer that is favorable for the type II process. Similarly, in α-alkyldeoxybenzoins, the phenyl ring directs the conformational preference in the cavity (Scheme 3). Such a hypothesis is supported by the results on dealuminated zeolite-Y, in which the Si to Al ratio is very high (>550). At very low levels of aluminum, the cation concentration is also low. Therefore, conformational control is expected to be minimal and, indeed, type I products dominate the product mixture in both the cases.

Wada et al. have investigated the photobehavior of iron pentacarbonyl included in a variety of alkali-exchanged Y zeolites [19]. Photocatalytic isomerization of *cis*-but-2-enes was investigated. Although the details of the mechanism are yet to be understood, the activity decreased with the decrease in the electrostatic field of the cation: Li-Y, 27.3; Na-Y, 18.7; K-Y, 1.22; Rb-Y, 0.45; and Cs-Y, 0.71 x 10^{-6} mol min^{-1}.

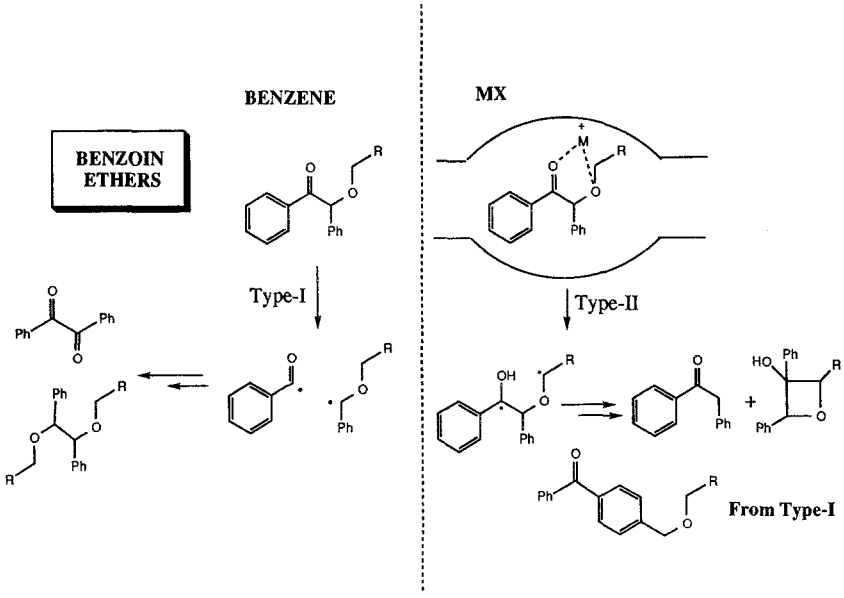

Scheme 2.

Table 3. Product distributions upon photolysis of benzoin methyl ether and α-propyldeoxybenzoin within zeolites[a].

Medium	Norrish Type I Products		Norrish Type II Products	
	Benzil/Pinacol ether	Rearrangement product	Deoxybenzoin	Cyclobutanol
(a) Benzoin methyl ether				
Benzene	26/67	1.0	1	7
Li-X	3	77	13	8
Na-X	4	72	10	14
K-X	7	48	14	18
Rb-X	5	46	18	22
Cs-X	8	34	17	31
(b) α-Propyldeoxybenzoin				
Benzene	5/24	--	54	17
Li-X	--	95	4	1
Na-X	--	88	5	7
K-X	--	48	31	21
Rb-X	--	32	22	45
Cs-X	--	21	27	42

a. Yields of products are based on GC analyses; see Schemes 2 and 3 for structure of products.

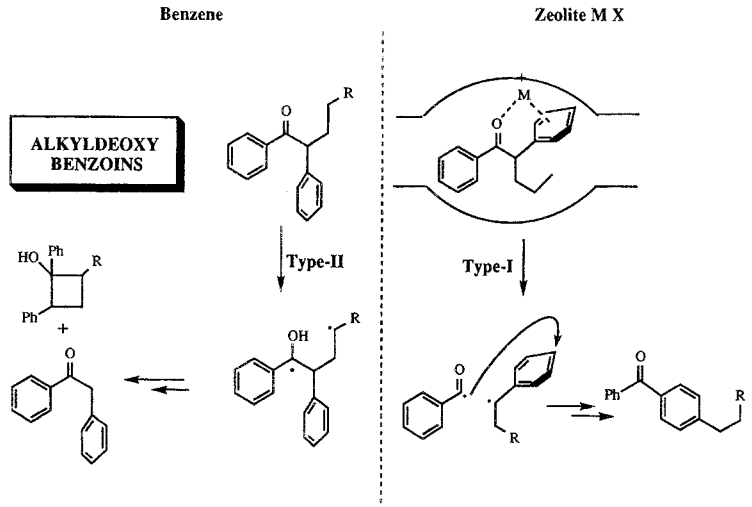

Scheme 3.

4. Guest-Cation Interaction: Heavy-Atom Effect

In the section above, we noted that light cations such as Li^+, Na^+, and K^+ interact strongly with guest molecules. A similar interaction, although more weakly, persists even with heavier cations such as Rb^+, Cs^+, and Tl^+. Weak interactions that exist between the cation and guest molecules lead to unique effects as illustrated in this section.

As shown in Figure 8, the emission spectrum of naphthalene is profoundly affected by inclusion in X and Y zeolites [20, 21, 22]. For low-mass cations such as Li^+ and Na^+, the emission spectra show the typical naphthalene blue fluorescence. However, as the mass of the cation increases (e.g., from Rb^+ to Cs^+ to Tl^+), there is a dramatic decrease in fluorescence intensity and a simultaneous appearance of a new vibronically structured low-energy emission band that is readily identified as naphthalene phosphorescence. Table 4 lists excited singlet (at 298 K) and triplet lifetimes (at 77 K) of naphthalene included within various cation-exchanged zeolites. It is clear that both these lifetimes are cation dependent. On the basis of the following observations, we conclude that the heavy-cation effect is responsible for the enhanced phosphorescence and decreased singlet and triplet lifetimes for naphthalene within K-, Rb-, Cs-, and Tl-cation-exchanged faujasites. It is well known that the effect of external heavy-atom perturbation scales with the square of the perturber's spin-orbit coupling constant, ξ^2 and that a log-log plot of τ_T^{-1} vs. ξ^2 should be linear with a predicted maximum slope of unity [23]. As shown in Figure 9, the expected dependence is observed. For comparison, we have also provided in Figure 9 the linear relationship observed in two systems, namely 1-halonaphthalenes [23] and 1,5-naphtho-22-crown-6 [24], where the external and internal heavy-atom effects, respectively, are presumed to operate. The magnitude of the heavy-atom effect observed in zeolites is significantly larger than that observed for the 1,5-naphtho-22-crown-6 exchanged with heavy-atom cations where the cation is rigidly held over the naphthalene π-face. In fact, the zeolite samples show heavy-atom effects nearly as large as for a series of 1-halonaphthalenes where the perturbers are covalently attached to the chromophore. This is attributable both to the close approach between naphthalene and the heavy-atom which is enforced by the zeolite supercage and to the presence of more than one heavy-atom cation per supercage which leads to highly effective concentrations of the heavy-atom cation in the vicinity of the naphthalene molecule. If the heavy-cation effect is indeed responsible for the variations in singlet and triplet lifetimes, one would expect a linear relationship between singlet- and triplet-decays with cation variation. Indeed, this is observed. The slope of the line suggests that the singlet-decay is enhanced more than the triplet, consistent with the smaller energy gap between the S_1 and T_1 as compared to the T_1 and S_0.

In order to obtain a picture of the geometry of the cation-aromatic (naphthalene) interaction in X- and Y-type faujasites, we took advantage of the heavy-atom induced phosphorescence which allows the use of optical detection of magnetic resonance (ODMR) in zero applied magnetic field [25]. The sublevel specific dynamics for absorbed naphthalene show a distinct increase in relative radiative character and total rate

constant of the out-of-plane x-sublevel with increasing mass of the cation perturber. Enhancement from only triplet sublevel T_x is expected for a heavy-atom approach along the x-axis [26]. ODMR kinetic results suggests that the naphthalene is absorbed through its π-cloud at a cation site (Figure 10).

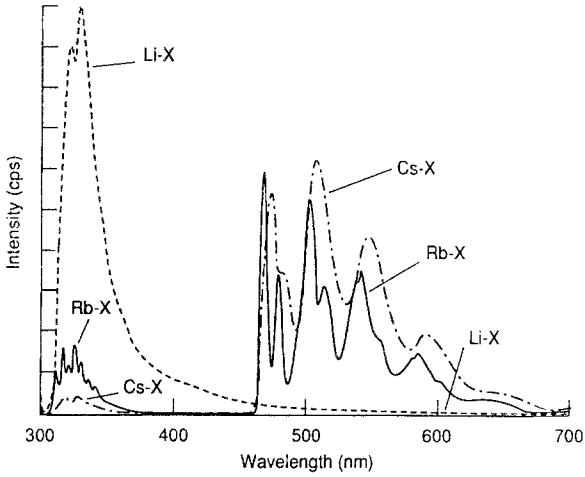

Figure 8. Emission spectra of naphthalene included in various cation–exchanged X zeolites. The ratio of fluorescence to phosphorescence depends on the cation.

Table 4. Photophysical parameters for naphthalene included within zeolites.

Zeolite Host	Triplet Lifetime[a] (s)	Singlet Lifetime[b] (ns)	P/F[c]
Li-X	-	33.0	1.0×10^{-4}
Na-X	-	35.4	7.3×10^{-2}
K-X	1.72	19.4	0.16
Rb-X	0.72	2.22	8.1
Cs-X	0.20	0.23 (87%), 1.87 (13%)	45
Tl-X	0.0012	—	only P
Li-Y	-	31.8	1.2×10^{-3}
Na-Y	-	25.1	1.0×10^{-3}
K-Y	-	13.8	0.1
Rb-Y	-	3.8	9.0
Cs-Y	-	0.7	60

a. The lifetime measured at 77 K.

b. The lifetime measured at 298 K.

c. Phosphorescence to fluorescence intensity ratio estimated at 77 K; the number is independent of the wavelength of excitation.

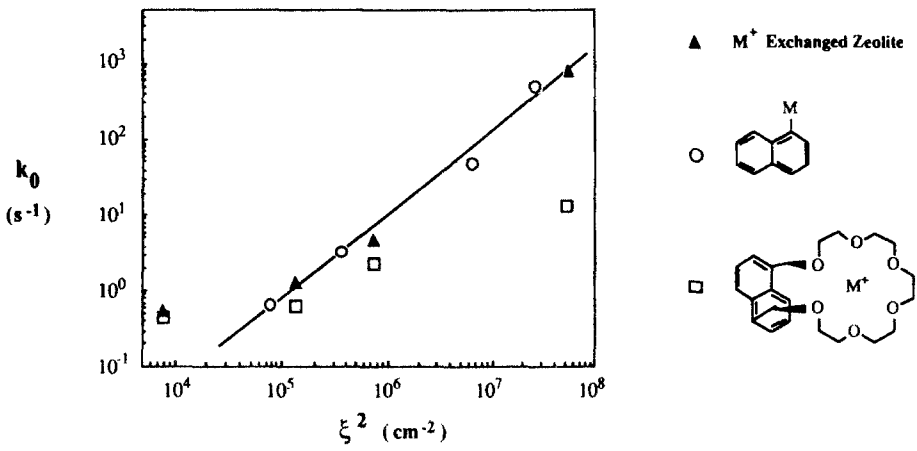

Figure 9. Correlation between the triplet decay and the spin–orbit parameter for naphthalene included in cation-exchanged zeolites. For comparison, results on other related systems are also shown.

The above heavy-cation effect within zeolites is found to be general. Enhanced phosphorescence is observed for a wide-range of different organic guests, such as anthracene, acenaphthylene, phenanthrene, chrysene, fluoranthene, pyrene, and 1,2,3,6,7,8-hexahydropyrene when included in Tl^+-exchanged faujasites (Figure 11). The only set of examples of guests for which phosphorescence is not observed are fused aromatics, which are too large in diameter to fit through the ~7.4 Å windows of the X- and Y-type zeolites (e.g., coronene and triphenylene). Also, this phenomenon is not restricted to faujasites alone. Enhanced phosphorescence has been observed for guest molecules within heavy-cation-exchanged zeolites ZSM-5, L, mordenite, omega, and beta.

It is easy to appreciate the potential of the unusual environment of the zeolite when one realizes that even olefins (Chart 2), systems that under normal conditions do not show phosphorescence, emit from their triplet states when included in Tl^+-exchanged zeolites.

Excitation of *trans*-stilbene included in Tl-X and in Tl-ZSM-5 emits phosphorescence and fluorescence both at room temperature and at 77 K [27]. The triplet emission spectra at 77 K for a number of substituted *trans*-stilbenes included in Tl-X are provided in Figure 12. The triplet emission maxima for stilbenes measured in the present study agree well with the literature reports [28]. The ability to record phosphorescence from stilbenes even at 298 K is significant as only very weak phosphorescence from *trans*-stilbene and several substituted *trans*-stilbenes has been recorded at 77 K in organic glass containing ethyl iodide as the heavy-atom perturber.

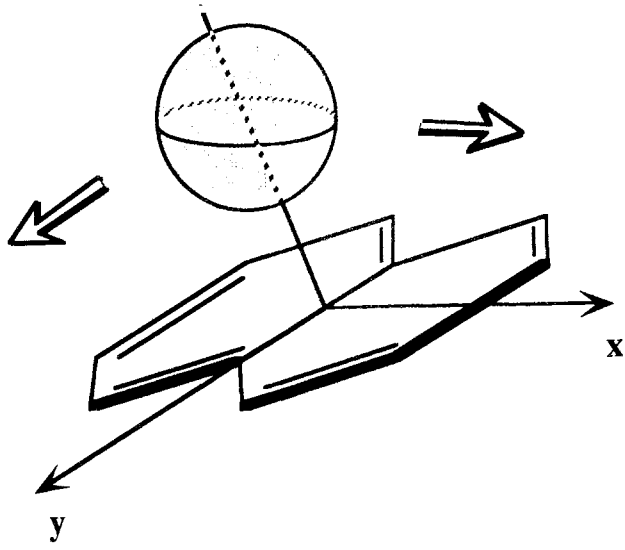

Figure 10. Geometry of cation-binding to naphthalene as inferred from ODMR experiments.

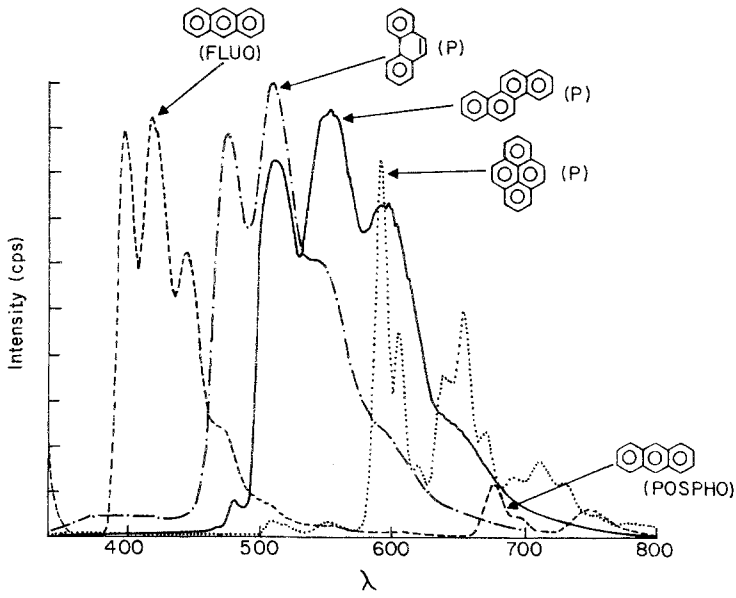

Figure 11. Emission spectra of aromatics included within Tl-X at RT. Emission consists mostly of phosphorescence.

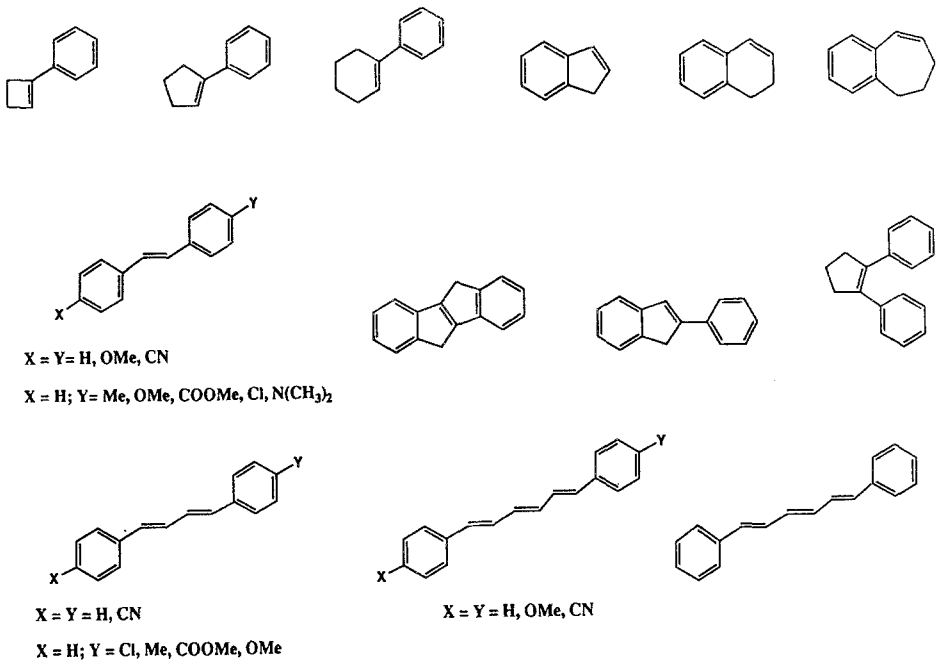

Chart 2.

In an effort to expand the utility of these zeolite hosts for the observation of phosphorescence from triplet states, we have investigated the photophysics of several 1-phenylcycloalkenes and phenyl-fused cycloalkenes included in thallium-exchanged zeolites. In Figures 13 and 14, the triplet emission spectra at 77 K of several 1-phenylcycloalkenes and phenyl fused cycloalkenes included in Tl-X are provided [27]. For compounds for which literature estimates are available, the 0—0 transition of the phosphorescence emission and the reported S_0 to T_1 absorption agree remarkably well (see inserts in Figures 13 and 14) [29].

All-*trans* α,ω-diphenylpolyenes exhibit very low intersystem crossing efficiencies and efficient fluorescence. To our knowledge, no authentic phosphorescence spectra from these have been reported. We have succeeded in recording phosphorescence of these α,ω-diphenylpolyenes by including them in Tl^+-exchanged zeolites [27]. Figure 15 shows the observed phosphorescence of the α, ω-diphenylpolyenes included in Tl-X. At 77 K, a well-resolved structured emission for each of the polyenes with a prominent vibronic spacing of 1200-1400 cm^{-1} (as expected for triplet phosphorescence) is observed. The singlet-triplet energy gaps ($\Delta_{T_1 \rightarrow S_0}$) obtained from the observed zero-zero lines are in excellent agreement with literature predictions [30].

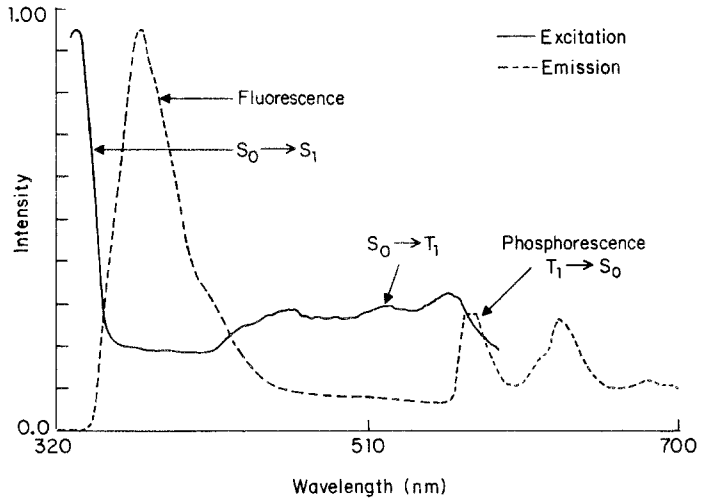

Figure 12. Emission and excitation spectra at 298 K of *trans*-stilbene included in Tl-X.

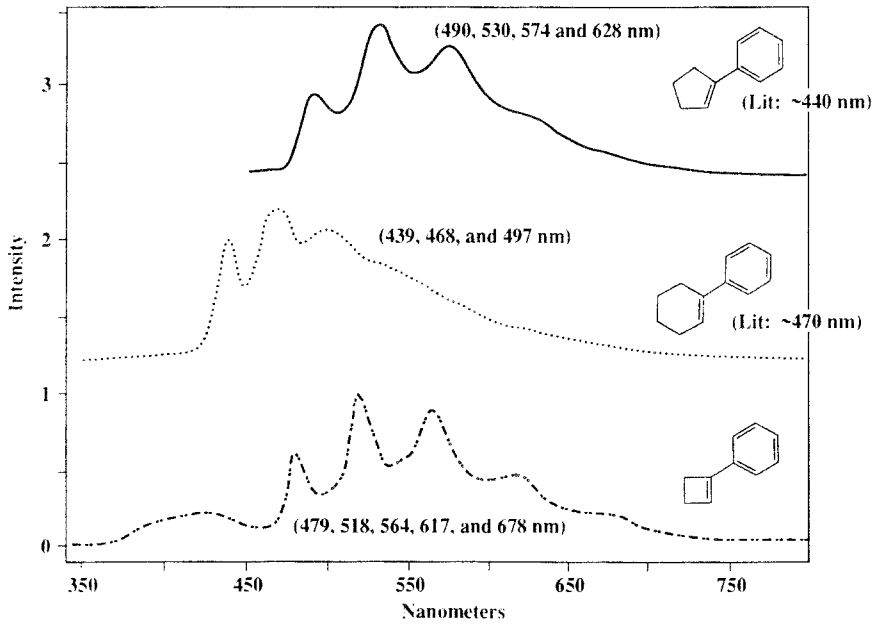

Figure 13. Phosphorescence spectra at 77 K of 1-phenylcycloalkenes included in Tl-X.

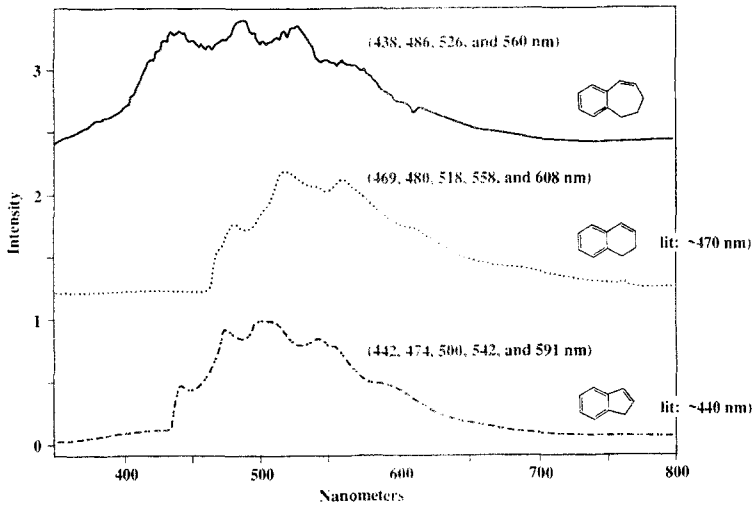

Figure 14. Phosphorescence spectra at 77 K of phenyl-fused cycloalkenes included in Tl-X.

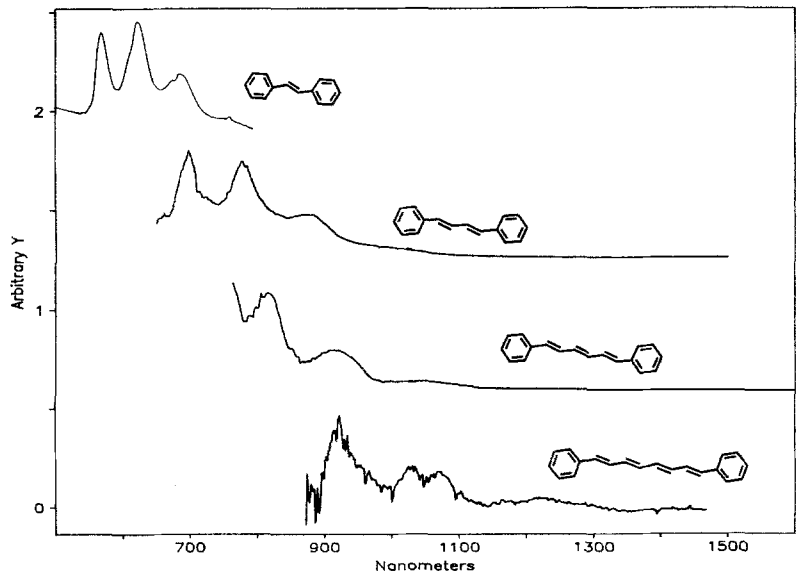

Figure 15. Phosphorescence spectra at 77 K of α,ω-diphenyl polyenes included in Tl-X. Excitation wavelength: stilbene, 295 nm; diphenylbutadiene, 340 nm; diphenylhexatriene, 350 nm; diphenyloctatetraene, 375 nm.

In addition to the above systems, enhanced cation-dependent phosphorescence from xanthone and *para*-dimethylaminobenzonitrile [31] included within ZSM-5 and Y zeolites has been observed recently.

As discussed above, cations can be utilized to control the efficiency of the triplet generation from an organic molecule included in the cavities of zeolites. Two examples provided below illustrates how such an effect can also be utilized to control product distribution in a photoreaction.

The photobehavior of acenaphthylene is unique in that it has been extensively studied in various constrained media and has been subjected to one of the largest heavy-atom effects on its dimerization [32]. The irradiation of acenaphthylene in solution yields the *cis*- and the *trans*-dimers; the singlet gives predominantly *cis*-dimer, whereas the triplet gives both *cis*- and *trans*-dimers in comparable amounts (Scheme 4). Photolyses of dry solid inclusion complexes of acenaphthylene in various cation (Li, Na, K, Rb)-exchanged Y zeolites gave the *cis*- and *trans*-dimers [33]. *Cis*- to *trans*-dimer ratio, relative efficiency of dimerization, relative triplet yields, and triplet lifetimes of acenaphthylene are dependent on the cation as summarized in Table 5.

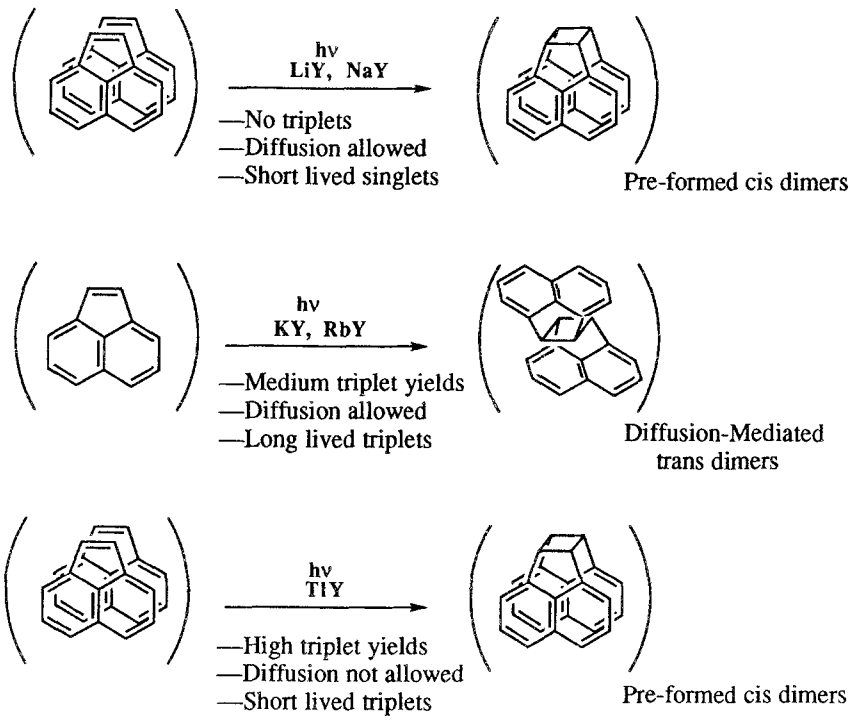

Scheme 4.

Table 5. Cation dependent photodimerization of acenaphthylene included in M^+-Y type zeolites (<S>=0.5)

Zeolite	*Cis*-/*Trans*-dimer Ratio	Relative Efficiency of Dimerization	Relative Triplet Yield	Triplet Lifetime (μs)
Li-Y	25	0.2	-	--
Na-Y	25	0.2	-	--
K-Y	2.3	0.4	0.2	9.6
Rb-Y	1.5	1.0	0.5	5.7
Cs-Y	4.2	0.8	0.7	2.1

The absence of triplet formation in Li-Y and Na-Y is consistent with the solution behavior in which the intersystem crossing yield from S_1 to T_1 is reported to be near zero. This, as well as the exclusive formation of *cis* dimer, support the conclusion that the dimerization in the supercages of Li-Y and Na-Y is from the excited singlet-state. The high triplet yield in K- and Rb-Y is thought to be a consequence of the "heavy-atom effect" caused by the cations present within the supercage. The trends observed in the variation of the triplet yield and the triplet lifetime with the increasing mass of the cation are consistent with the expected spin-orbit-coupling-induced triplet formation. Formation of the *trans*-dimer (the triplet-derived product) in the cages of K- and Rb-Y is in agreement with triplet generation.

Another example relates to unimolecular rearrangement of β,γ-unsaturated ketone (Scheme 5 and Table 6) [34]. This compound undergoes a 1,3-acyl shift from the excited singlet state and oxa-di-π-methane rearrangement from the triplet state. It is clear from Table 6 that the ratio of products derived via excited singlet and triplet states are dependent on the cation when irradiation of the ketone included in Y zeolite is carried out. Consistent with our suggestion that the triplet formation is enhanced in heavy-cation-exchanged zeolites, the singlet lifetime is decreased and the fluorescence to phosphorescence ratio is enhanced.

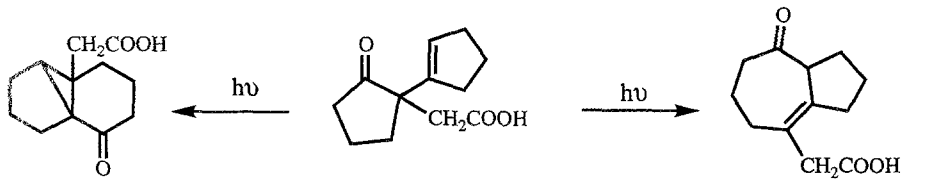

Triplet Product Singlet Product

Scheme 5.

Table 6. Photophysical properties[a,b] and photochemical behavior of β,γ-unsaturated ketone (Scheme 5).

Zeolite	Singlet to Triplet Product Ratio	F/P[c]	S_1 lifetime at 77 K (ns)
Li-Y	>99:1	10:1	9.2
Na-Y	>99:1	10:1	8.9
K-Y	58:42	5:1	8.2
Rb-Y	47:53	2:1	6.9
Cs-Y	82:18	2:1	5.8
Tl-Y	38:62	0.2:1	4.4

a. Two emissions one with short lifetime (ns range; λ_{max}: 378 nm) and the other with long lifetime (ms range; λ_{max}: 430 nm) were recorded at 77 K. Both emissions had the same excitation spectra at 77 K. At room temperature the longer wavelength emission was absent. Short wavelength emission was attributed to the S_1 state and the long wavelength one to the T_1 state.

b. The singlet lifetimes were measured at 77 K on an Edinburgh single photon counting spectrometer.

c. Fluorescence to phosphorescence ratio at 77 K.

5. Guest-Cation Interaction: Acid-Base Interaction

Zeolites possess a number of acidic and basic sites. When the exchangeable cation is proton, Brønsted acid sites are also present. The strength of Lewis basic sites (12-ring oxygens in the windows of the supercages) in X and Y zeolites are known to be dependent on the cation. For example, in the case of Y-type zeolites, it has been estimated that the negative charge on the 12-ring oxygen atoms increases with the decrease in cation acidity (Li-Y, -0.345; Na-Y, -0.351; and K-Y, -0.381) [35]. Among a number of techniques, fluorescence has been popular in monitoring the surface acidity of zeolites [36]. Fluorescence probes such as 8-quinolinol, 8-hydroxyquinoline, quinoline, α- and β-naphthols, and acridine are used to measure the Brønsted surface acid strengths. Surface acidity is estimated from the emission intensities of neutral and acidic or basic forms. Lewis as well as Brønsted acid sites on the surfaces of zeolites have been monitored with pyridine. In all of these cases, interaction between the acid sites and the probe results in a new emitting species such as protonated probe, charge transfer complex, or species resulting from electron transfer from the probe to the Lewis site.

Three examples provided below illustrate the importance of considering the possibility of acid-base interactions when organic molecules are included within zeolites:

Benzophenone included within cation- (H^+, Li^+, Na^+, K^+, Rb^+, and Cs^+) exchanged ZSM-5 yields phosphorescence characteristic of both protonated and hydrogen-bonded forms [37]. The ratio of these emissions depends on the temperature of zeolite activation and the nature of the cation. Smaller cations such as Na^+ and H^+ favor the protonated form. It is suggested that the cation changes the surface acidity and larger cations such as Rb^+ and Cs^+ do not favor the formation of free proton.

Irradiation of *trans*-azobenzene included within H^+-Y and H^+-β zeolites, yields a

cyclization product benzo[c]cinnoline and a disproportionation product benzidine (Scheme 6) [38]. These products are not obtained upon irradiation in a neutral medium and in Na-Y. Formation of these products within zeolites is suggested to result from the protonated form of azobenzene.

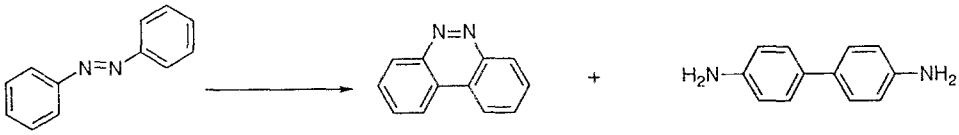

Scheme 6.

Cozens, Garcia, and Scaiano have shown recently that the photobehavior of 1,1-diphenyl-2-propanone within zeolites (Na-Y and in H-Y) depends on the availability of protons [39]. α-Cleavage is the primary process in both cases but the resulting products when 1,1-diphenyl-2-propanone is included in Na-Y and in H-Y are different (Scheme 7). Differing final products result from the fact that reacting species under the two conditions are different–in one case it is the neutral species whereas in the other it is the protonated form.

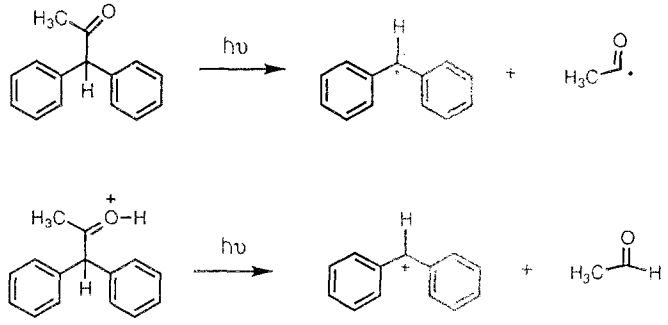

Scheme 7.

6. Cations as Reaction Cavity Free Volume Controllers: Lebensraum Effect

In the sections above, zeolites are considered to have active reaction cavities. However, several early studies pointed out that they do possess cavities which are passive in character with respect to certain reactions. We illustrate below with several examples why the cations, under certain circumstances should be considered nothing more than

inert fillers which reduce the free volume available for the reactants within zeolites.

Irradiation of dibenzylketone in unrestricted environments such as solution media is characterized by the formation of benzyl radicals following α-cleavage and decarbonylation processes [40,41]. The termination process of these radicals is generally the uncorrelated (random) coupling to yield 1,2-diphenylethane. Photolysis of unsymmetrically substituted derivatives (represented as A(C=O)B), results in the formation of three radical coupling products, AA, AB and BB, in a ratio of 1:2:1 (Scheme 8). In contrast, when escape of the radicals is impeded by confining environments, the radical recombination probability is modified by favoring the formation of geminate products of the AB type. It has also been observed that recombination of the primary radical pair can sometimes occur before decarbonylation (or escape) giving rise to rearranged ketone photoproducts and recovered starting material (Schemes 8 and 9) [42]. Recombination of the primary radical pair generates 1-phenyl-*ortho*-methyl acetophenone (o-MAP) and 1-phenyl-*para*-methyl-acetophenone (p-MAP) by *ortho*- and *para*-coupling, respectively, in the case of DBK. Thus, in using DBKs as probes, one measures the yields of diphenyl ethanes and rearranged products and, in certain cases, the isotope enrichment factor (see below). The cage-effect, defined as {AB-(AA+BB)/(AA+AB+BB)}, is a measure of restriction (a factor dependent on topology) and is calculated from the yields of diphenyl ethanes. The isotope enrichment factor, (α), defined as {rate of disappearance of ^{12}C ketone/rate of disappearance of ^{13}C ketone}, is measured from quantum yields of disappearance of the ^{12}C and ^{13}C ketones.

The results obtained upon photolysis of evacuated samples of DBK under conditions of a relatively low loading (2% w/w) (which represents a nominal occupancy of ~15%) in the cation-exchanged X and Y zeolites are shown in Table 7. The first important observation comes from the fact that the product distribution depends significantly on the cation in the M-X zeolites while it remains relatively constant in the M-Y zeolite series.

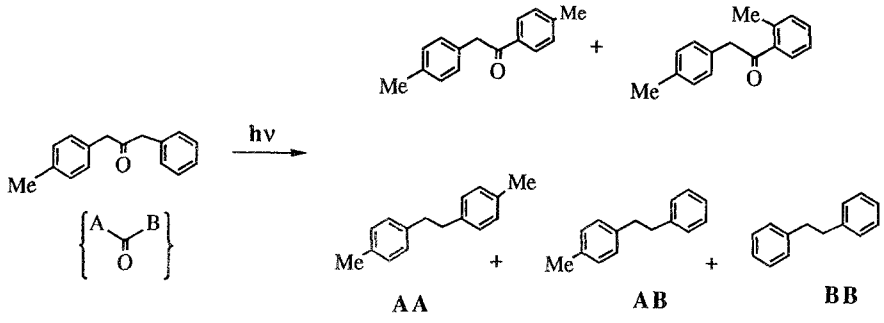

Scheme 8.

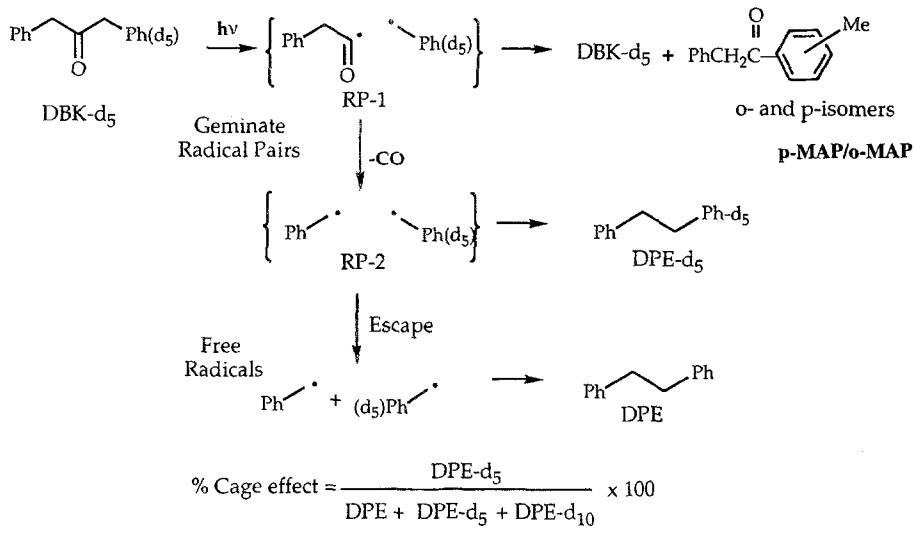

Scheme 9.

The results of the cage-effect obtained with isotopically labelled, DBK-d_5 at 2% w/w loading (~15 % occupancy), are also shown in Table 7 [43]. The yields of DPE-d_5, DPE-d_{10}, and DPE-d_0 determined by GCMS were used to calculate the cage-effect (Scheme 9). The most important observation relating to cage-effect is that the cage-effect increases from Li- to K- in the M-X zeolites, and that it remains constant in the M-Y zeolite series.

The magnetic field and magnetic isotope effects in the M-X and M-Y zeolites have been analyzed by examining the product distribution from isotopically labelled (^{13}C and ^{2}H) DBK in faujasites both at the earth's magnetic field and at 2000 G [44]. The results presented in Table 8 can be summarized as follows: (1) there is no difference in the product ratio (within the experimental error) for any of the variables for the M-Y and Li-X zeolites, (2) there are significant ^{13}C and ^{2}H isotope and magnetic field effects upon photolysis in Na-X, (3) there is a significant magnetic field effect on the product ratio for photolysis of DBK in K-X (even though there is no magnetic isotope effect), and (4) the results observed with DBK-d_{10} closely parallel the results observed with ^{13}C-DBK.

Trends in product distribution, cage-effects, and magnetic field effects observed with M-X and M-Y zeolites are consistent with the paradigm that the reaction cavity free volume controls the reaction profile and that is dependent on the size and number of cations present within the supercages [44]. In the case of Li-X and M-Y zeolites,

substantial yields of decarbonylation products, relatively modest cage effects (Table 7) and small amounts of rearranged products (0-20%) emphasize the importance of the globally closed zeolite spaces. The lack of magnetic field and magnetic isotope effects in the products of primary radical recombination are also consistent with a relatively large space where the radical centers can separate and explore the global environment. In contrast, in K-X zeolites, large yields of rearranged products are obtained. Large magnetic field effects and no magnetic isotope effect in this zeolite are consistent with most coupling reactions occuring in a tight local environment where escape is difficult and enforced orbital overlap is important. These results suggest that spin-orbit coupling, which is isotope independent, may be the intersystem crossing mechanism in K-X zeolites. Finally, in agreement with our expectations, photolyses in Na-X give evidence of an environment that is intermediate between that observed in Li-X and M-Y on one hand, and K-X on the other. The local inter-radical distance and the ease of escape are expected to be intermediate between them. As the local space is also expected to be larger, intersystem crossing can be controlled by nuclear-electron hyperfine couplings (which are isotope dependent) as well as by strong external magnetic fields.

The product distribution obtained upon photolysis of benzoin alkyl ethers, α-alkyldeoxybenzoins, and α-alkyldibenzyl ketones is dependent on the cation as summarized in Tables 3 and 9 with one example from each class [18, 45, 46]

Table 7. Product distribution[a] and cage-effect from photolysis of DBK (2% w/w) in ion-exchanged faujasites (Schemes 8 and 9).

	Percentage Yield			
Zeolite	DPE	*o*-MAP	*p*-MAP	Cage Effect[b]
Li-X	80	3	16	5
Na-X	55	17	26	22
K-X	40	40	16	73
Li-Y	100	0	0	19
Na-Y	95	0	5	17
K-Y	94	2	4	19

a. Calculated error limit, 10%.

b. Cage-effect measured under the same conditions in a separate experiment by using DBK-d_5.

Photoprocesses undertaken by benzoin ethers and deoxybenzoins are shown in Scheme 2. In solution, the termination process of the benzyl radicals derived from α-alkyldibenzyl ketones consists only of the coupling between the two benzylic radicals and results in diphenylalkanes AA, AB, and BB in a statistical ratio of 1:2:1. Scheme 10 provides the structure of products and a mechanism for the formation of these products.

Within supercages, on the other hand, termination proceeds by both coupling and disproportionation (Table 9). A schematic diagram for the termination processes between the benzylic radicals is shown in Scheme 11. Preference for disproportionation within the supercage has been interpreted as follows: the association between benzylic radicals which would favor coupling, would be prohibited inside the cavity, especially in the presence of large cations, because of the reduction in free volume. Further, more drastic overall motion would be required to bring benzylic radicals together for head-to-head coupling than to move an alkyl group so that one of its methylene hydrogens would be in a position for abstraction by the benzylic carbon radical. It is logical to expect the radical pair to prefer the pathway of "least volume and motion" when the free space around it is small. Thus, as smaller cations are replaced with larger ones and as shorter alkyl chains are replaced with longer ones, one would indeed expect enhanced yields of olefins as observed in the reported study (Figure 16).

Table 8. Magnetic isotope and field effects on the product distribution from photolysis of DBK in M-X zeolites (Schemes 8 and 9)[a]

System	Percentage Yield		
	DPE	*o*-MAP	*p*-MAP
Li-X			
DBK-^{12}CO	81 [85][c]	3 [3]	16 [12]
DBK-^{13}CO (90%)[b]	81 [85]	3 [2]	16 [13]
DBK-d_{10} (95%)	79	2	19
Na-X			
DBK-^{12}CO	56 [65]	17 [13]	26 [22]
DBK-^{13}CO (90%)	27 [33]	37 [25]	36 [42]
DBK-d_{10} (95%)	67 [59]	10 [13]	23
K-X			
DBK-^{12}CO	40 [68]	40 [14]	16 [18]
DBK-^{13}CO (90%)	45 [62]	32 [13]	20 [25]
DBK-d_{10} (95%)	45	35	20

a. Results for M-Y zeolites are similar under all conditions (90–100% yield of DPE and very little isomers).

b. Isotope content of the sample.

c. Bracketed number is the product yield in the presence of 2000 G external magnetic field.

Table 9: Product distribution upon photolysis of α-hexyl dibenzyl ketone within zeolites[a].

	Percentage of		
Medium	Olefin	(AB)	Rearrangement Product
Li-X	39	17	37
Na-X	19	18	57
K-X	23	29	36
Rb-X	38	23	29
Cs-X	60	15	22

a. see Scheme 10 for structures.

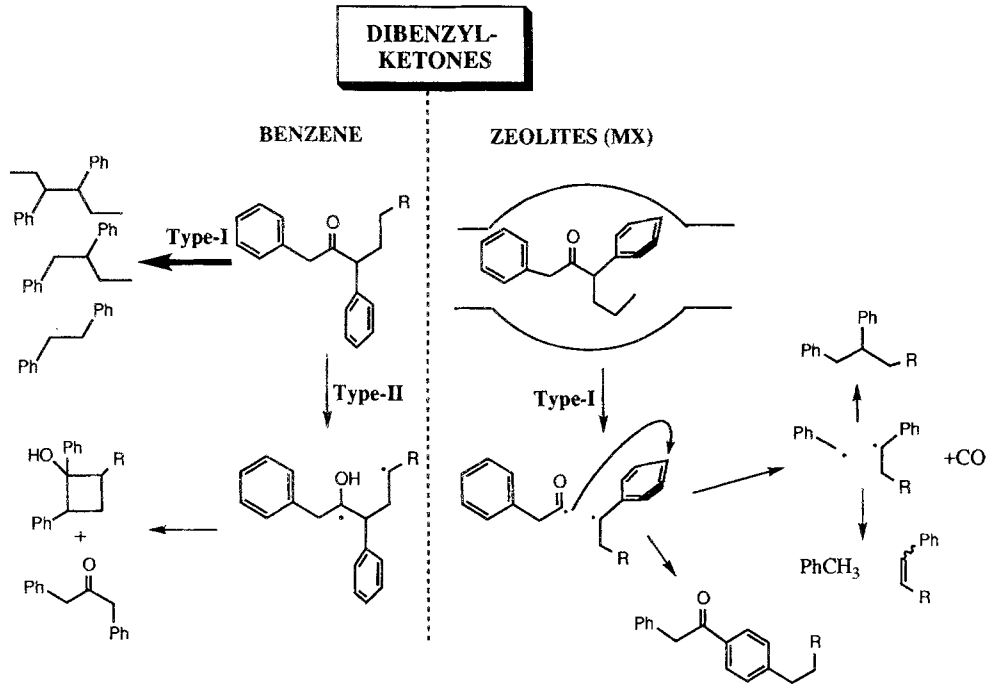

Scheme 10.

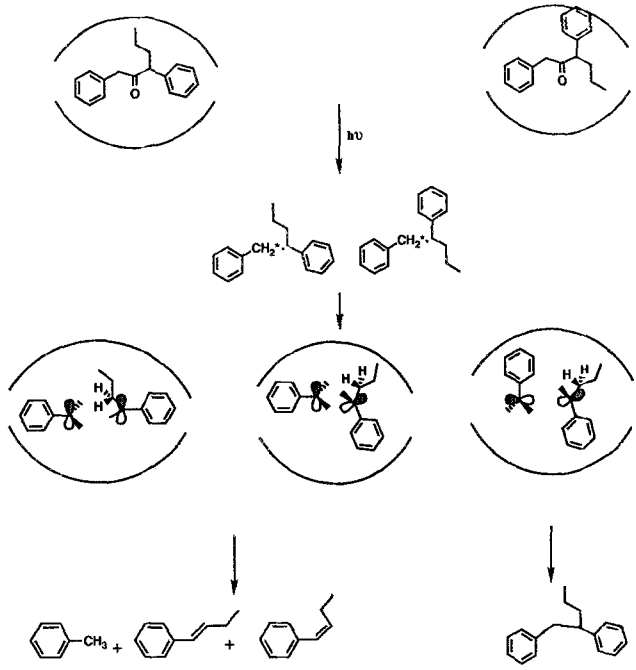

Scheme 11.

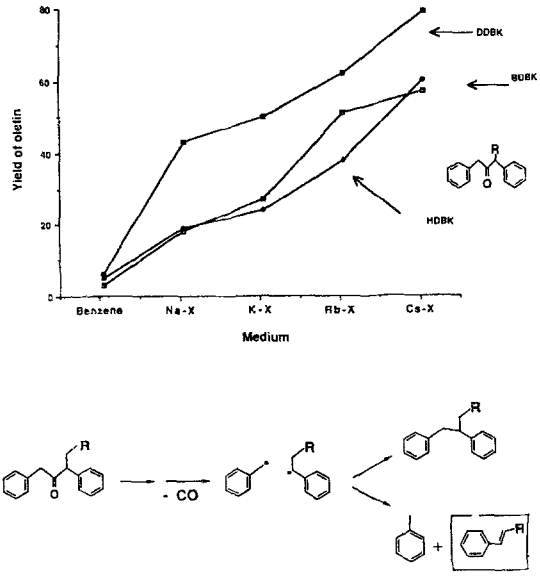

Figure 16. Photolysis of α-alkyl dibenzylketone: product dependence on cation.

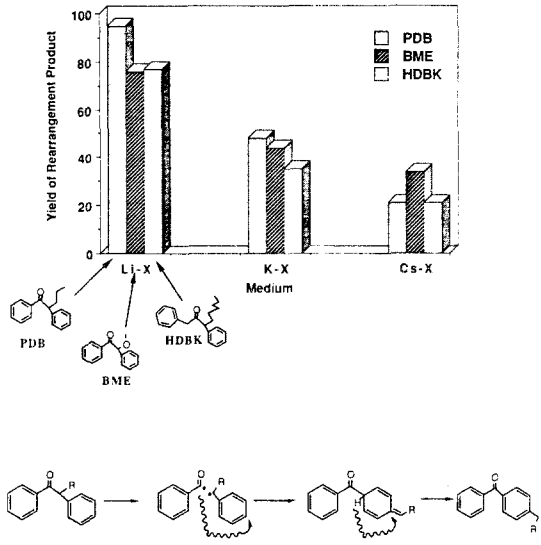

Figure 17. Photolysis of alkyldeoxybenzoin: cation dependent product distribution.

The above conclusion is also supported by the pathways undertaken by the primary triplet radical pair (Scheme 10) generated by the α-cleavage of the α-alkyl dibenzyl-ketones and α-alkyl benzoin ethers and deoxybenzoins (Schemes 2 and 3). Perusal of Tables 3 and 9 reveals that while the rearrangement takes place in all cation-exchanged X and Y zeolites, the yield of the rearrangement product varies depending on the cation (Figure 17). The yield decreases as the cation present in the supercage is changed from Li^+ to Cs^+. Such a trend is attributed to the decrease in the free space within the supercage. As the available free space inside the supercage is decreased by the increase in the size of the cation, the translational and rotational motions required for the rearrangement process become increasingly hindered (Scheme 12). Under these conditions, competing paths, such as coupling to yield the starting ketone and decarbonylation, both of which require less motion, dominate. Examination of Table 3 reveals that in the case of α-methylbenzoin ether as well as in α-propyldeoxybenzoin the C/E ratio, i.e., the ratio of the yield of cyclobutanol, the cyclization (C) product, to that of deoxybenzoin, the elimination product (E) resulting from the 1,4-diradical derived via the Norrish type II γ-hydrogen abstraction process, depends on the cation present in the supercage. Also, the C/E ratio increases as smaller cations are replaced with the larger ones, i.e., C/E increases from Li^+ to Cs^+. The above dependence of the product

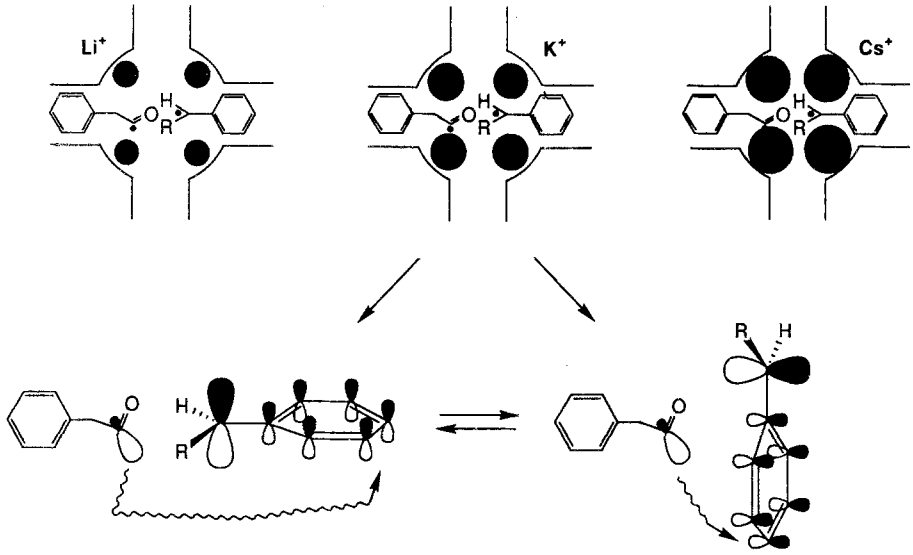

Scheme 12.

distribution on the cation can be understood on the basis of the well-understood mechanism of the type II reaction. The enhancement of cyclization within the supercages of X and Y zeolites in the presence of larger cations is believed to reflect the rotational restriction brought on the skewed-*transoid-cisoid* 1,4-diradical inter-conversion (Scheme 13). We propose that as the cation size increases, the 1,4-diradical is forced to adopt a compact geometry due to reduction in the available supercage free volume. Thus, the skewed 1,4-diradical first formed would be encouraged to relax to the *cisoid-* rather than to the *transoid-* conformer. Severe constraints would be imposed by the supercage on the *cisoid-transoid* interconversion and the barrier for the *cisoid* to *transoid* conversion would be accentuated. These factors are expected to enhance the yield of cyclobutanol.

One final example under this category deals with the photo-Fries rearrangement of phenyl benzoate [47]. As shown in Scheme 14 , irradiation of phenyl benzoate in polar and non-polar solvents yields *ortho-* and *para-* isomers almost in equal amounts. However, irradiation of phenyl benzoate included in X and Y zeolites yields the *ortho*-isomer preferentially (Table 10). A clear trend in the *ortho-para* ratio with respect to cation is evident both in X and Y zeolites. Increasing size of the cation reduces the chances of the benzoyl fragment migrating to the *para*-position. Consistent with the paradigm presented above reduction in the *ortho-para* ratio is much larger in X than in Y zeolites. Smaller cations with larger numbers (X zeolites) do the same job, reduce the free volume, as larger cations with fewer numbers (Y zeolites). Thus, from the examples above, it is clear that one has a handle on the size of the nanoreactors where the photoreaction is conducted.

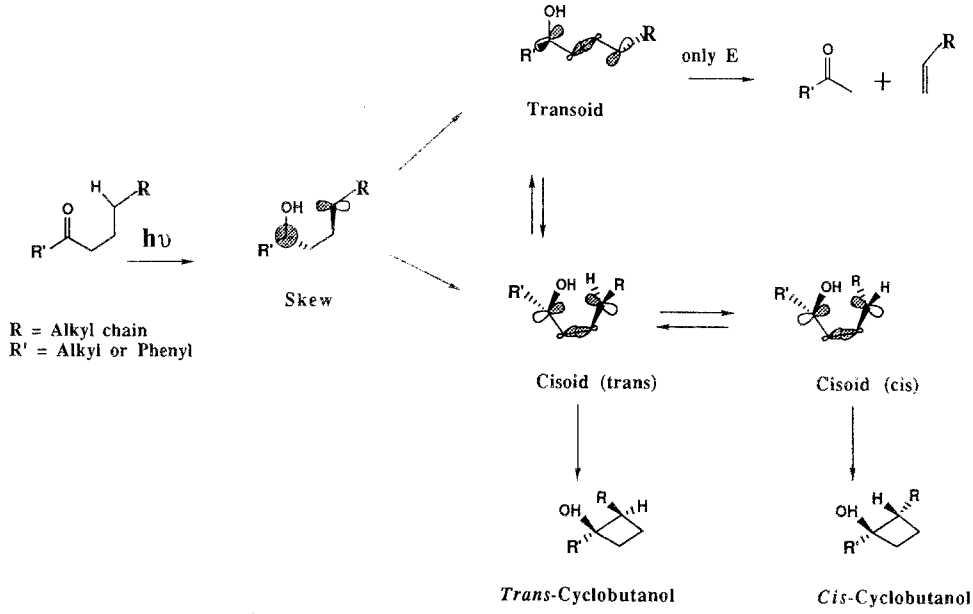

Scheme 13.

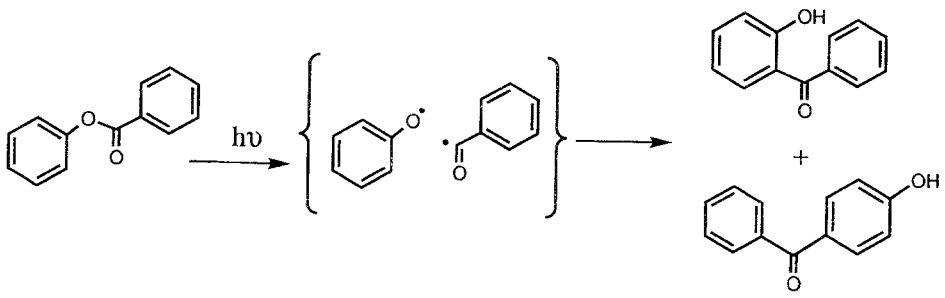

Scheme 14.

Table 10: Photolysis of phenylbenzoate in M-Y zeolites: effect of cation on the rearrangement process — *ortho*-, *para*-isomers (Scheme 14).[a]

Medium/Zeolite	Percentage of *ortho*-isomer	Percentage of *para*-isomer	Percentage of phenol
Hexane	49	37	14
Benzene	53	38	8
Methanol	49	43	6
Li-Y	91	8	1
Na-Y	93	6	1
K-Y	98	-	2
Rb-Y	98	-	2
Cs-Y	97	-	3

a. All zeolite irradiations were conducted as slurries in hexane. After two hour photolysis products were extracted with ether and analyzed by gc.

7. Role of Hydrated Cations

The discussions above are concerned with anhydrous zeolites wherein the cations can be considered to be "naked". These cations are free to interact with the guest molecules. However, it is well known that zeolites are highly hygroscopic and the absorbed water molecules are co-ordinated to the cations present within supercages. In this section, we discuss how the presence of water within zeolite supercages alters the photochemical and photophysical behavior of guest molecules.

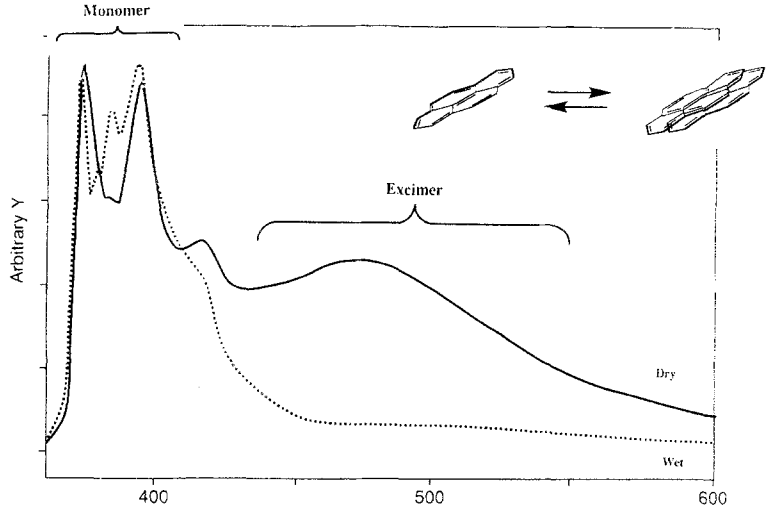

Figure 18. Influence of water on the emission spectra of pyrene included in Na-Y zeolites.

Excitation of pyrene included within anhydrous Na-Y results in two emissions as shown in Figure 18, one from the monomer and the other from the excimer [48]. The so-called excimer emission is definitely not an emission from typical dynamic excimer, since the excitation spectra for the monomer and the excimer emissions are different (Figure 19). An obvious choice of the latter emission being due to microcrystals was ruled out on the basis of following observations: (a) Both the wavelengths of emission and excitation are not identical to those of crystals reported in the literature; (b) The internal void space of Na-Y is too small to accommodate microcrystals; however, if micro-crystals are formed on the external surfaces they should be washable with excess hexane. Hexane wash did not change the ratio of intensities of emission from monomer and excimer. These observations suggested that the excimer results from pre-aggregated dimers (static excimers) present within the supercages of Na-Y. Such a conclusion is also supported by the following observations: (a) No growing-in of the excimer in the nanosecond time scale was noticed when the excimer emission decay was monitored by time resolved single photon counting techniques; (b) No negative pre-exponential term for excimer decay was obtained; (c) The ratio of the intensities of excimer to monomer emission increased slightly upon lowering the temperature; (d) Variation of loading level between 0.002 and 0.2 (average number of molecules per supercage) did not alter the pyrene monomer lifetime significantly.

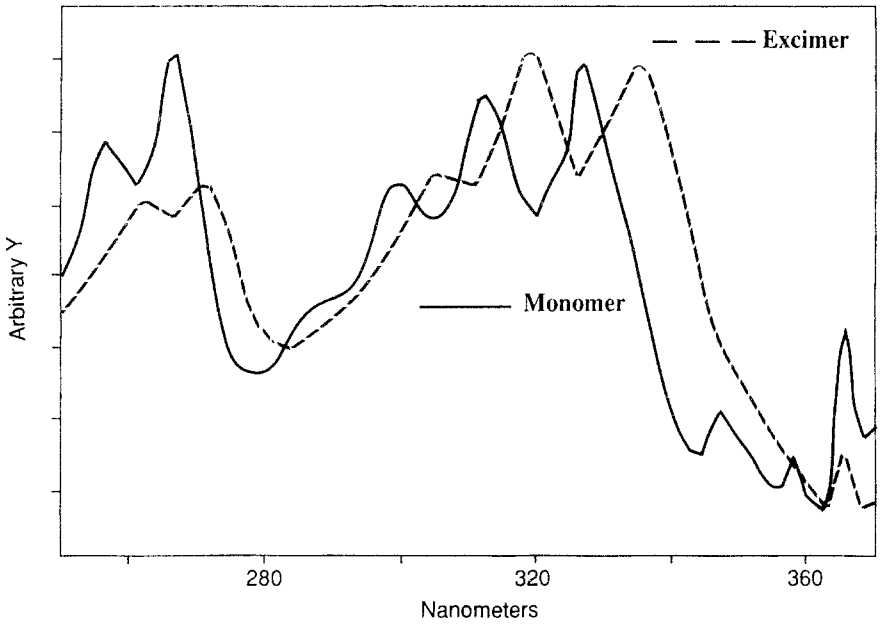

Figure 19. Excitation spectra for the monomer and excimer emissions of pyrene included within "dry" Na-Y: (a) ——, monomer, em l: 380 nm; (b) – – –, excimer, em l: 480 nm.

Co-absorption of water has a striking influence on the nature of aggregation of pyrene within zeolites. As seen in Figure 18, the intensity of excimer emission from pyrene present within fully hydrated Na-Y is fairly low. In fact, there is a correlation between the ratio of intensities of monomer to excimer emissions and the water content (Figure 20). Decrease in excimer emission with the increase in water content indicates that pre-aggregation is not favored within "wet" zeolites. Such may be the result of reduction in polarizing power of the cation; pre-aggregation is proposed to be a result of polarization of pyrene molecules by the cation (Figure 21).

The photophysical properties of phenanthrene bring out yet another unique characteristic of guest occupancy distribution with respect to water content within zeolites [49]. Emission spectra of phenanthrene included within anhydrous zeolite is non-unique (<S> varied between 0.002 to 0.1); fluorescence from the monomer is detected and no excimer emission is seen. However, when the zeolite containing higher loadings of phenanthrene (<S> above 0.1) absorbs water, in addition to the monomer emission, fluorescence from microcrystals is detected (Figure 22). A change in the occupancy status (monomer to microcrystals) is also reflected in diffuse reflectance spectra. At lower loading levels (<S> lower than 0.1), independent of the hydration status emission spectra corresponded only to that of the monomer and diffuse reflectance spectra of both wet and dry samples were nearly identical.

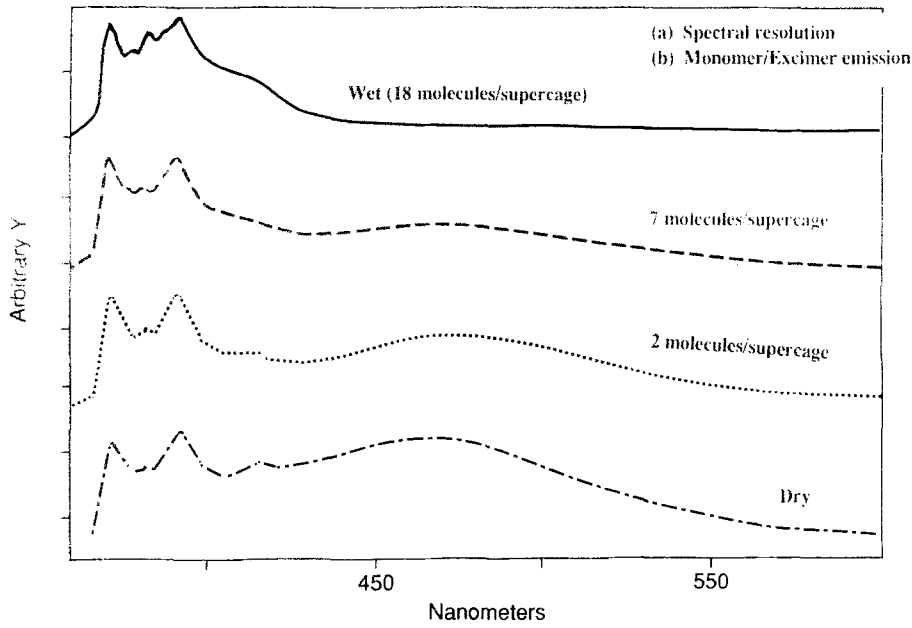

Figure 20. Emission spectra (excitation l: 340 nm) of pyrene within Na-Y at various loading levels of co-absorbed water: (a) – · – · –, "dry", no water; (b) · · · · · ·, <S>: 2; (c) – – – – –, <S>: 7; (d) ———, <S>: 18.

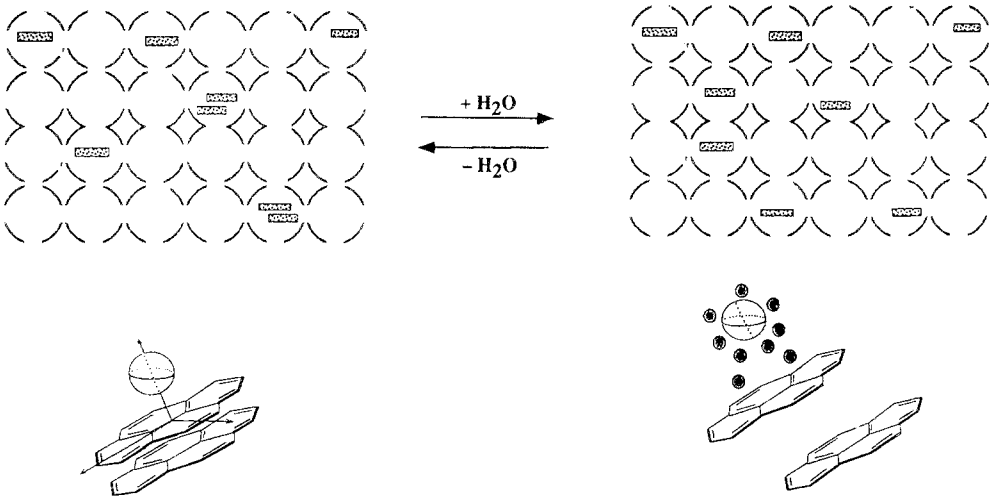

Figure 21. A schematic illustration of the influence of water on pyrene aggregation. Cation interaction leads to polarization of pyrene.

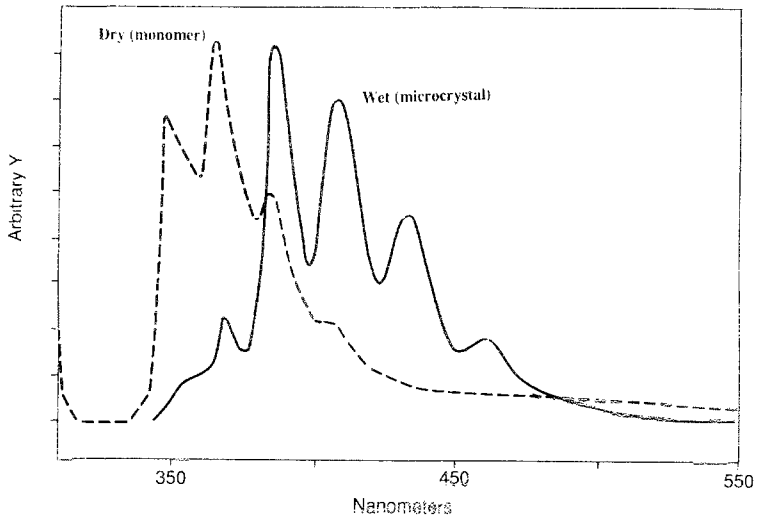

Figure 22. Emission spectra of phenanthrene, <S>: 0.4, included within "dry" and "wet" Na-Y: (a) - - - -, "dry" Na Y, ex l: 293 nm; (b) ———, "wet" Na-Y, ex l: 320 nm.

The association of phenanthrene to form micro-crystals at higher loadings is believed to be prompted by displacement of phenanthrene, by water, from the internal to external surface. At low loading levels of phenanthrene, apparently both water and phenanthrene are able to co-exist within the internal surfaces of Na-Y. When the wet zeolite containing phenanthrene was washed with excess hexane, the hexane wash contained significant amounts of phenanthrene. However, similar wash of anhydrous zeolite containing phenanthrene did not result in phenanthrene loss into the hexane layer. This suggested that the location of phenanthrene under the two conditions (wet and dry) are different. Under anhydrous conditions, phenanthrene is absorbed into the zeolite whereas, when the zeolite is hydrated, at least part of phenanthrene is adsorbed onto the outer surface (which is washable with hexane), i.e., microcrystals are located on the external surfaces of Na-Y. When the above hexane-washed, wet phenanthrene,Na-Y complex was subjected to dehydration-hydration cycle, no emission due to micro-crystals was detected indicating that excess phenanthrene which could not be accommodated (at high loadings) in presence of co-absorbed water has been removed by initial hexane wash. What was most unique was that when the unwashed hydrated sample was dehydrated, emission due to microcrystals completely disappeared and only monomer emission was detected. Thus dehydration-hydration cycles promote monomer-microcrystal cycles.

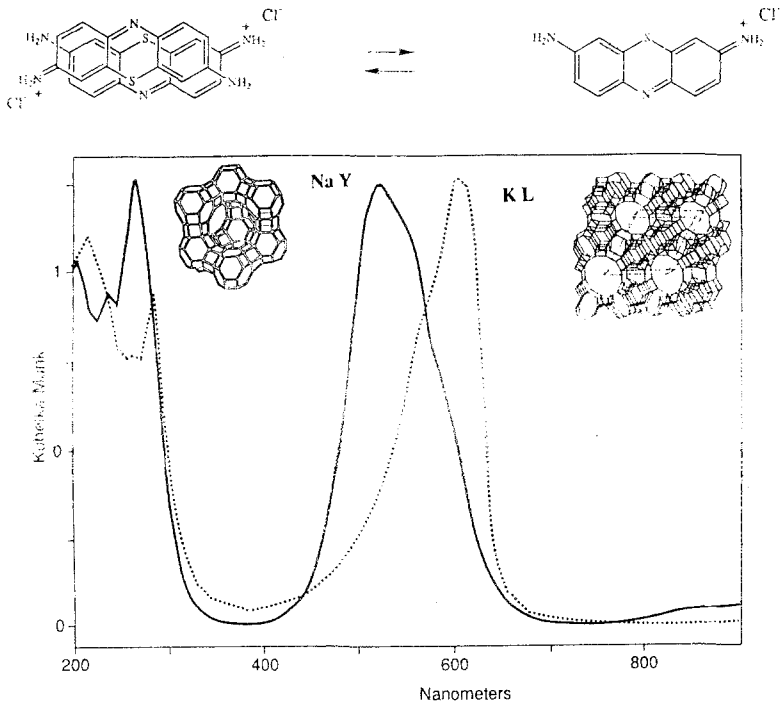

Figure 23. Diffuse reflectance spectra of thionin included within dry K-L and Na-Y.

In another interesting study within zeolites, the control of aggregation of dyes by co-absorbed water has also been observed [50]. Among the dyes studied were methylene blue, oxazine170, nile blue A, acridine orange, and cresyl violet. With thionin as an example, it was shown that complexation can be achieved from aqueous solutions by cation exchange. Thionin possesses a delocalized positive charge and is capable of partially displacing (ca 5%) Na^+ and K^+ from Y- and L-type zeolites. The dye-exchanged Y and L zeolites were shown to have different spectroscopic properties assigned to the state of aggregation of the dye (Figure 23). While monomeric thionin displays a strong absorption maximum at about 610 nm, dimeric thionin, also referred to as H-dimers, absorbs at about 540 nm. On visual inspection, thionin-exchanged K-L-zeolites appear pink while thionin exchanged Na-Y zeolites appear blue. These results suggest that the formation of thionin aggregation is not possible within the straight channel structure of L-zeolites. While the ~7.5Å diameter of L-zeolite channels may accommodate thionin molecules along their long axis, they seem unable to accommodate the face-to-face H-aggregated dimers. Complexation of thionin in the larger supercages of the Na-Y zeolites, on the other hand, results in the formation of hydrated H-dimer-complexed zeolites. It was also found that dehydration of the zeolite complex under high vacuum at moderate temperatures resulted in no change in the L-zeolite but displaced the

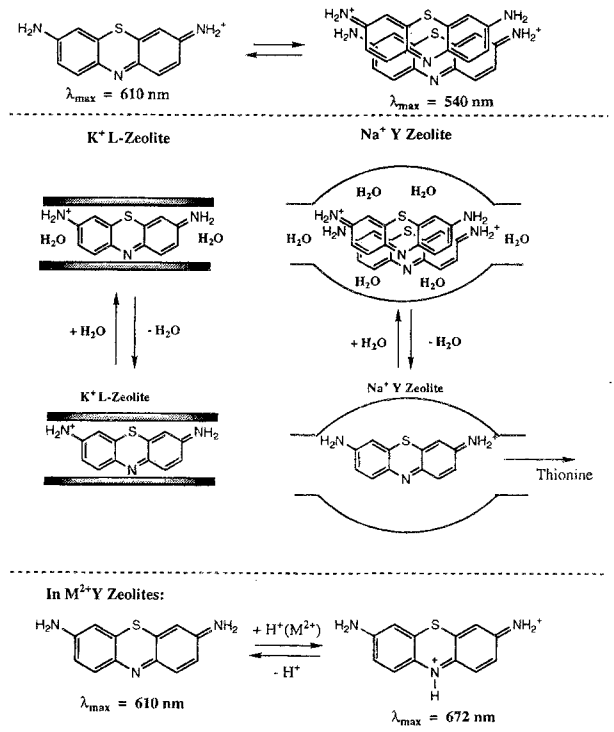

Scheme 15.

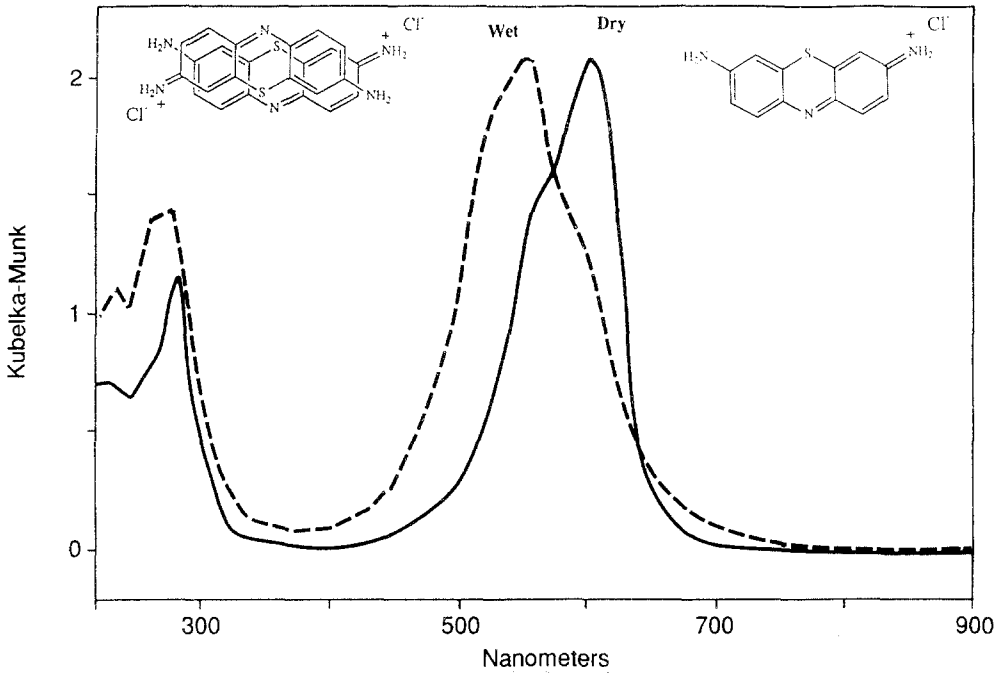

Figure 24. Diffuse reflectance spectra of thionin included within Na-Y: effect of included water.

equilibrium towards the monomeric state of the dye in the Y-zeolites (Scheme 15 and Figure 24). It was shown that aggregation in Y-zeolites depends on the concentration of the dye and on the nature of the exchangeable cation. No aggregate formation was observed when the number of thionin molecules per supercage was lower than 0.0005 or with Cs-Y zeolites, which are known to posses a very small free volume in the supercages. Divalent cations, such as Mg^{2+}, Ca^{2+}, and Sr^{2+}, displayed a behavior that was similar to that of Na-Y until water concentrations were lower than ca. 3%. Under those conditions, the formation of protonated thionin chromophores was observed suggesting that removal of the last traces of water resulted in the formation of free H^+.

We close this section with two examples in which water influences the photochemical product formation [51,52]. As discussed previously, photochemistry of dibenzyl ketones is influenced within zeolites. Results of photolyses of dibenzylketone included in M-X zeolites under dry and wet conditions are tabulated in Table 11. It is clear that when water is present within the supercages, the rearrangement process is completed inhibited. The cage effect in the case of *para*-methyldibenzylketone is reduced to 8% under hydrated conditions from 40% in anhydrous Na-X zeolites. When water-content is varied methodically, it is evident that much of the influence occurred with 4 or 5 molecules of water per supercage (note that the supercage can accommodate as many as 28 molecules of water).

Table 11. Photolysis of dibenzylketone in M-X zeolites: effect of hydration[a].

Zeolite	Condition	Percentage		
		DPE	*o*-MAP	*p*-MAP
Li-X	Dry	81	3	16
	Wet	100	0	0
Na-X	Dry	55	17	26
	Wet	100	0	0
K-X	Dry	40	40	16
	Wet	98	1	1

a. See scheme 9 for product structures.

A similar observation was made during photolysis of alkanophenones within Na-X zeolites. As illustrated in Figure 25, the ratio of cyclization to elimination products of the 1,4-biradical is influenced by the number of water molecules present within supercages. We believe that the first few molecules of water that enter the supercages coordinate to the cations and that these are the ones which have maximum influence on reactions.

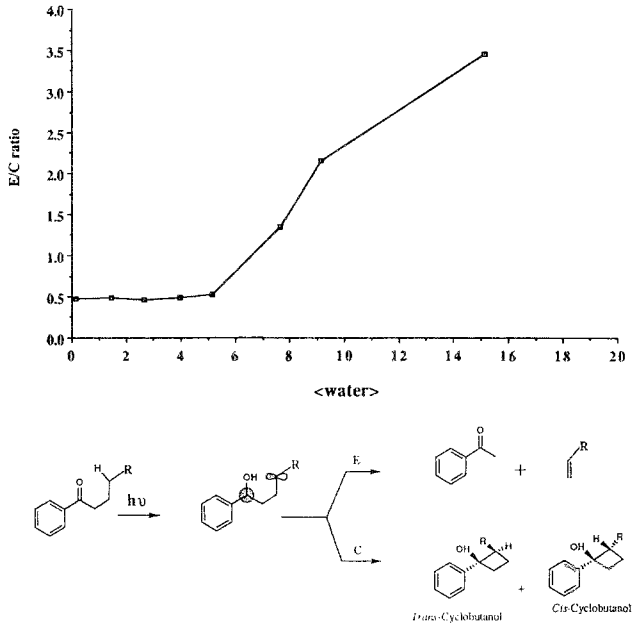

Figure 25. Influence of water on the elimination to cyclization product ratio from the 1,4-diradical resulting via γ-hydrogen abstraction in the case of valerophenone.

Molecules of water that come in afterwards merely fill the supercages. Further work is needed to understand this process. Water molecules that are present within the supercages interact with the hydroxyl of the 1,4-biradical and prevent internal return of the hydrogen and also influence the *transoid-cisoid* equilibrium of the diradical (Scheme 16).

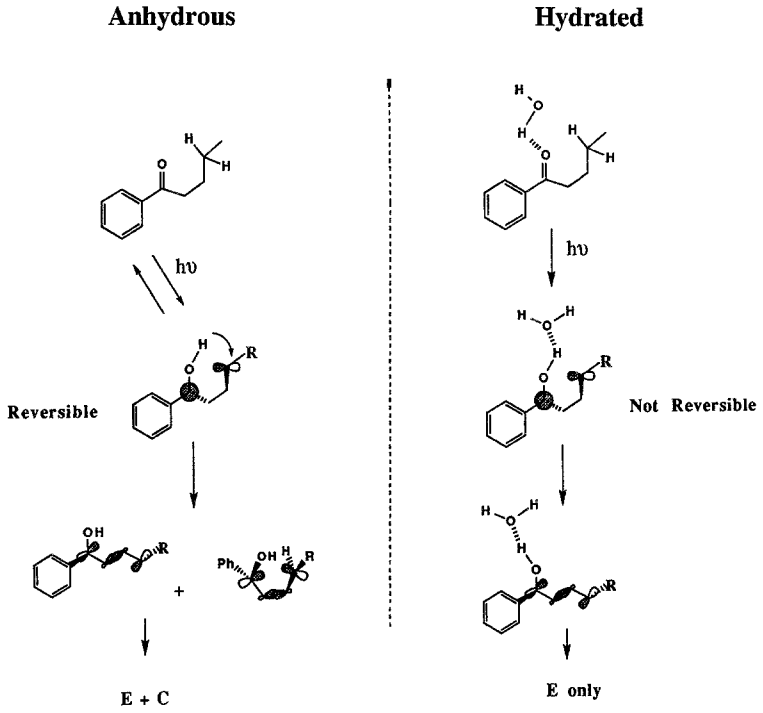

Scheme 16.

8. Summary

The influence of cations on the photochemical and photophysical processes described in this chapter clearly points out the need to understand the nature of the interaction between the cation and the guest molecules in order to predict the behavior of guests within zeolites. The role of cations in catalysis is yet to be addressed. Photophysical and photochemical studies of the type described in this article are expected to play an important role in the future towards understanding the role of cations in a number of thermal processes in which zeolites play an unique catalytic role.

Acknowledgment: VR thanks Tulane University for financial support and NJT thanks the National Science Foundation and the Air Force Office of Scientific Research for their generous support of this research.

References

1. K. Kalyanasundaram, *Photochemistry in Microheterogeneous Systems*, Academic Press, New York (1987);
   T. Matsuura and M. Anpo (Eds), *Photochemistry on Solid Surfaces*, Elsevier, Amsterdam (1989);
   V. Ramamurthy (Ed), *Photochemistry in Organized and Constrained Media*, VCH, New York (1991);
   H.-J. Schneider, and H. Durr (Eds), *Frontiers in Supramolecular Organic Chemistry and Photochemistry*, VCH; Weinheim (1991);
   V. Balzani and F. Scandola, *Supramolecular Photochemistry*, Ellis Horwood, Chichester, England (1991).
2. V. Ramamurthy, R. G. Weiss, and G. S. Hammond, *Adv. Photochem.*, **18**, 67 (1993).
3. N. J. Turro and P. Wan, *Tetrahedron Letters*, **25**, 3655 (1984);
   H. L. Casal and J. C. Scaiano, *Can. J. Chem.*, **62**, 628 (1984);
   S. L. Suib and A. Kostapapas, *J. Am. Chem. Soc.*, **106**, 7705 (1984).
4. For a summary see:
   N. J. Turro, *Pure & Appl. Chem.*, **58**, 1219 (1986);
   N. J. Turro, in *Molecular Dynamics in Restricted Geometries*, J. Klafter and J. M. Drake (Eds), John Wiley, New York, p 387 (1989);
   V. Ramamurthy, in *Photochemistry in Organized and Constrained Media*, V. Ramamurthy (Ed), VCH, New York, p 429 (1991);
   N. J. Turro and M. Garcia-Garibay, in *Photochemistry in Organized and Constrained Media*, V. Ramamurthy (Ed), VCH, New York, p 1 (1991);
   V. Ramamurthy, D. F. Eaton, and J. V Caspar, *Acc. Chem. Res.*, **25**, 299 (1992);
   V. Ramamurthy, *Chimia*, **46**, 359 (1992);
   P. Kamat, *Chem. Rev.*, **93**, 267 (1993);
   J. K. Thomas, *Chem. Rev.*, **93**, 301 (1993);
   K. B. Yoon, *Chem. Rev.*, **93**, 321 (1993);
   V. Ramamurthy and D. F. Eaton, *Chem. Materials*, **6**, 1128 (1994).
5. D. W. Breck, *Zeolite Molecular Sieves: Structure, Chemistry, and Use*, John Wiley and Sons, New York (1974);
   A. Dyer, *An Introduction to Zeolite Molecular Sieves*, John Wiley and Sons, Bath (1988);
   H. van Bekkum, E. M. Flanigen and J. C. Jansen (Eds), *Introduction to Zeolite Science and Practice*, Elsevier, Amsterdam (1991);

R. Szostak, *Molecular Sieves. Principles of Synthesis and Identification*, Van Nostrand, New York (1989).

6. D. W. Breck, *Zeolite Molecular Sieves: Structure, Chemistry, and Use*, John Wiley and Sons, New York, pp 529-592 (1974).
7. W. M. Meier and D. H. Olson, in *Atlas of Zeolite Structure Types*, Butterworths, Cambridge (Second Revised Edition), pp 96–97 (1987);
   R. Szostak, *Handbook of Molecular Sieves*, Van Nostrand Reinhold, New York, pp 183–188 (1992).
8. Calculations of polyhedral volumes were performed using a modification of the POLYVOL Program [D. Swanson and R. C. Peterson, *The Canadian Mineralogist,* **18**, 153 (1980); D. K. Swanson and R. C. Peterson, "POLYVOL Program Documentation", Virginia Polytechnic Institute, Blacksburg, VA] assuming the radius of the TO_2 unit to be 2.08Å (equivalent to that of quartz).
9. R. G. Weiss, V. Ramamurthy, and G. S. Hammond, *Acc. Chem. Res.*, **26**, 530 (1993).
10. M. Hepp, V. Ramamurthy, D. R. Corbin, and C. Dybowski, *J. Phys. Chem.*, **96**, 2629 (1992).
11. V. Ramamurthy, *Mol. Cryst. Liq. Cryst.*, **240**, 53 (1994).
    V. Ramamurthy, D. R. Sanderson, and D. F. Eaton, *J. Phys. Chem.*, **97**, 13380 (1993).
12. V. Ramamurthy and J. V Caspar, *Mol, Cryst. Liq. Cryst.*, **211**, 211 (1992).
13. Y. S. Liu, P. de Mayo, and W. R. Ware, *J. Phys. Chem.*, **97**, 5987, 5995 (1993).
14. V. Ramamurthy, D. R. Corbin, and L. J. Johnston, *J. Am. Chem. Soc.*, **114**, 3870 (1992).
15. E. J. Baum, J. K. S. Wan, and J. N. Pitts, *J. Am. Chem. Soc.*, **88**, 2652 (1966);
    D. R. Kearns and W. Case, *J. Am. Chem. Soc.*, **88**, 5087 (1966);
    A. A. Lamola, *J. Chem. Phys.*, **47**, 4810 (1967);
    P. J. Wagner, A. E. Kemppainen, and H. Schott, *J. Am. Chem. Soc.*, **95**, 5604 (1973).
16. V. Ramamurthy, D. R. Sanderson, and D. F. Eaton, *Photochem. Photobiol.*, **56**, 297 (1992).
    V. Ramamurthy and D. F. Eaton, in *Proceedings of the 9th International Zeolite Conference*, R. von Ballmoos, J. B. Higgins and M. M. J. Treacy (Eds), Butterworth-Heinemann, Boston, p 587 (1992).
17. V. Ramamurthy, D. R. Corbin, N. J. Turro, and Y. Sato, *Tetrahedron Lett.*, **30**, 5829 (1989);
    V. Ramamurthy, X. G. Lei, N. J. Turro, T. R. Lewis, and J. R. Scheffer, *Tetrahedron Lett.*, **32**, 7675 (1991).
18. D. R. Corbin, D. F. Eaton, and V. Ramamurthy, *J. Am. Chem. Soc.*, **110**, 4848 (1988).
19. Y. Wada, Y. Yoshizawa, and A. Morikawa, *J. Chem. Soc., Chem. Commun.*, 319 (1990).

20. V. Ramamurthy, J. V Caspar, E. W. Kuo, D. R. Corbin, and D. F. Eaton, *J. Am. Chem. Soc.*, **114**, 3882 (1992).
21. J. V. Caspar, V. Ramamurthy, and D. R. Corbin, *Coordination Chem. Rev.*, **97**, 225 (1990).
22. V. Ramamurthy, J. V. Caspar, D. R. Corbin, and D. F. Eaton, *J. Photochem. Photobiol. A: Chemistry*, **50**, 157 (1989).
23. M. Kasha, *J. Chem. Phys.*, **20**, 71 (1952);
D. S. McClure, *J. Chem. Phys.*, **17**, 905 (1949).
24. J. M. Larson and L. R. Sousa, *J. Am. Chem. Soc.*, **100**, 1942 (1978);
S. Ghosh, M. Petrin, A. H. Maki, and L. R. Sousa, *J. Chem. Phys.*, **87**, 4315 (1987);
S. Ghosh, M. Petrin, A. H. Maki, and L. R. Sousa, *J. Chem. Phys.*, **88**, 2913 (1988).
25. V. Ramamurthy, J. V. Caspar, D. R. Corbin, B. D. Schlyer, and A. H. Maki, *J. Phys. Chem.*, **94**, 3391 (1990).
26. G. Weinzierl and J. Friedrich, *Chem. Phys. Lett.*, **80**, 55 (1981).
27. V. Ramamurthy, J. V Caspar, E. W. Kuo, D. R. Corbin, and D. F. Eaton, *J. Am. Chem. Soc.*, **114**, 3882 (1992);
V. Ramamurthy, J. V Caspar, and D. R. Corbin, *Tetrahedron Letters*, **31**, 1097 (1990).
28. J. Saltiel, G. E. Khalil, and K. Schanze, *Chem. Phys. Lett.*, **70**, 233 (1980);
D. F. Evans, *J. Chem. Soc.*, 1351 (1957);
R. H. Dyck and D. S. McClure, *J. Chem. Phys.*, **36**, 2326 (1962);
H. Gorner, *J. Phys. Chem.*, **93**, 1826 (1989).
29. T. N. Ni, R. A. Caldwell, and L. A. Melton, *J. Am. Chem. Soc.*, **111**, 457 (1989);
P. M. Crosby, J. M. Dyke, J. Metcalfe, A. J. Rest, K. Salisbury, and J. R. Sodeau, *J. Chem. Soc., Perkin II*, 182 (1977).
30. G. Heinrich, G. Holzer, H. Blume, and D. Schulte-Frohlinde, *Z. Naturforsch.*, **25b**, 496 (1970);
D. F. Evans and J. N. Tucker, *J. Chem. Soc., Faraday Trans. II*, **68**, 174 (1972).
31. V. Ramamurthy and D. R. Sanderson, unpublished results.
32. D. O. Cowan and R. L. Drisko, *Elements of Organic Photochemistry*, Plenum, New York, p 435 (1976).
33. V. Ramamurthy, D. R. Corbin, C. V. Kumar, and N. J. Turro, *Tetrahedron Lett.*, **31**, 47 (1990).
34. B. Borecka, A. D. Gudmundsttir, G. Olovsson, V. Ramamurthy, J. R. Scheffer, and J. Trotter, *J. Am. Chem. Soc.*, **116**, 10322 (1994).
35. D. Barthomeuf, *J. Phys. Chem.*, **88**, 42 (1984).
36. For a review: A. M. Eremenko, *Adsorbtsiya Adsorbenty*, **8**, 48 (1980).
37. S. Okamoto, H. Nishiguchi, and M. Anpo, *Chem. Lett.*, 1009 (1992).
38. A. Corma, H. Garcia, S. Iborra, V. Marti, M. A. Miranda, and J. Primo, *J. Am. Chem. Soc.*, **115**, 2177 (1993).
39. F. L. Cozens, H. Garcia, and J. C. Scaiano, *J. Am. Chem. Soc.*, **115**, 11134 (1993).

40. (a) N. J. Turro, *Proc. Natl. Acad. Sci.*, **80**, 609 (1983);
(b) G. F. Lehr and N. J. Turro, *Tetrahedron*, **37**, 3411 (1981);
(c) N. J. Turro and B. Kraeutler, *Acc. Chem. Res.*, **13**, 369 (1980).
41. (a) P. S. Engel, *J. Am. Chem. Soc.*, **92**, 6074 (1970);
(b) W. K. Robins and R. H. Eastman, *J. Am. Chem. Soc.* , **92**, 6076 (1970).
42. N. J. Turro and G. C. Weed, *J. Am. Chem. Soc.*, **105**, 1861 (1983).
43. Z. Zhang, Ph.D Thesis, Columbia University (1989)
44. N. J. Turro and Z. Zhang, *Tetrahedron Letters*, **30**, 3761 (1989)..
45. V. Ramamurthy, D. R. Corbin, and D. F. Eaton, *J. Org. Chem.* **55**, 5269 (1990).
46. D. R. Corbin, D. F. Eaton, and V. Ramamurthy, *J. Org. Chem.*, **53**, 5384 (1988); V. Ramamurthy, D. R. Corbin, D. F. Eaton, and N. J. Turro, *Tetrahedron Lett.*, **30**, 5833 (1989).
47. K. Pitchumani and V. Ramamurthy, unpublished results.
48. V. Ramamurthy and D. R. Sanderson, *J. Phys. Chem.*, **97**, 13380 (1993).
49. V. Ramamurthy, *Mol. Cryst. Liq. Cryst.*, **240**, 53 (1994).
50. V. Ramamurthy, D. R, Sanderson, and D. F. Eaton, *J. Am. Chem. Soc.*, **115**, 10438 (1993).
51. Z. Zhang and N. J. Turro, unpublished results.
52. V. Ramamurthy and D. R. Sanderson, unpublished results.

Abstract. In this article, we illustrate how one can utilize the cation embedded in a zeolite matrix to control the photophysical and photochemical behavior of guest molecules included in zeolite cages/cavities. Three aspects of cation-guest interaction are highlighted. Strong electronic interaction between the cation and the guest leads to mobilization of guests within zeolite supercages, alteration of the lowest electronic configuration ($n\pi^*$, $\pi\pi^*$) and restriction of conformation of molecules. Less obvious to a non-photochemist is the ability of cations, depending on their atomic weight, to induce spin conversion (singlet-triplet) in molecules. Photophysical studies carried out with aromatics and photodimerization of acenaphthylene highlight this point. The power of the heavy-atom cation effect in zeolites has been demonstrated by recording phosphorescence from several olefins whose phosphorescence has not previously been recorded. Cations by their sheer size can influence the mobility of molecules within zeolites. Restriction of motion of reactive intermediates results in product selectivity in reactions as illustrated with a few examples. Properties of cations and consequently their influence can change depending on whether they are hydrated or uncoordinated to water. Aggregation of dyes and aromatics and reactivities of carbonyl compounds are influenced by water present within zeolites. We have shown in this article that zeolites can be used as unique reaction vessels for photochemical reactions.